Shergottites Dhofar 019, SaU 005, Shergotty, and Zagami: ^{40}Ar-^{39}Ar chronology and trapped Martian atmospheric and interior argon

Ekaterina V. KOROCHANTSEVA[1, 2], Mario TRIELOFF[1*], Alexei I. BUIKIN[1, 2], and Jens HOPP[1]

[1]Institut für Geowissenschaften, Ruprecht-Karls-Universität Heidelberg, Im Neuenheimer Feld 236, D-69120 Heidelberg, Germany
[2]Vernadsky Institute of Geochemistry, Kosygin St. 19, 119991 Moscow, Russia
*Corresponding author. E-mail: trieloff@min.uni-heidelberg.de

Abstract–We report a high-resolution ^{40}Ar-^{39}Ar study of mineral separates and whole-rock samples of olivine-phyric (Dhofar 019, Sayh al Uhaymir [SaU] 005) and basaltic (Shergotty, Zagami) shergottites. Excess argon is present in all samples. The highest (^{40}Ar/^{36}Ar)$_{trapped}$ ratios are found for argon in pyroxene melt inclusions (~1500), maskelynite (~1200), impact glass (~1800) of Shergotty and impact glass of SaU 005 (~1200). A high (^{40}Ar/^{36}Ar)$_{trapped}$ component—usually uniquely ascribed to Martian atmosphere—can also originate from the Martian interior, indicating a heterogeneous Martian mantle composition. As additional explanation of variable high (^{40}Ar/^{36}Ar)$_{trapped}$ ratios in shocked shergottites, we suggest argon implantation from a "transient atmosphere" during impact induced degassing.

The best ^{40}Ar-^{39}Ar age estimate for Dhofar 019 is 642 ± 72 Ma (maskelynite). SaU 005 samples are between 700–900 Ma old. Relatively high ^{40}Ar-^{39}Ar ages of melt inclusions within Dhofar 019 (1086 ± 252 Ma) and SaU 005 olivine (885 ± 66 Ma) could date entrapment of a magmatic liquid during early olivine crystallization, or reflect unrecognized excess ^{40}Ar components. The youngest ^{40}Ar-^{39}Ar age of Shergotty separates (maskelynite) is ~370 Ma, that of Zagami is ~200 Ma.

The ^{40}Ar-^{39}Ar chronology of Dhofar 019 and SaU 005 indicate <1 Ga ages. Apparent ages uncorrected for trapped (e.g., Martian atmosphere, mantle) argon components approach 4.5 Ga, but are not caused by inherited ^{40}Ar, because excess ^{40}Ar is supported by ^{36}Ar$_{trapped}$. Young ages obtained by ^{40}Ar-^{39}Ar and other chronometers argue for primary rather than secondary events. The cosmic ray exposure ages calculated from cosmogenic argon are 15.7 ± 0.7 Ma (Dhofar 019), 1.0–1.6 Ma (SaU 005), 2.1–2.5 Ma (Shergotty) and 2.2–3.0 Ma (Zagami).

INTRODUCTION

Mars is the only terrestrial planet from which we likely have rocky samples, the SNC (Shergotty, Nakhla, Chassigny-type) meteorites (e.g., Walker et al. 1979; Bogard and Johnson 1983; Becker and Pepin 1984; Swindle et al. 1986; McSween 1994; Meyer 2007). SNC meteorites provide important insights into Martian evolution and comparative planetology (e.g., McSween 1994). One key observation arguing for a Martian origin are the young radioisotopic ages of most SNC meteorites, which requires an active, large parent planet with an extended geologic activity—although a recent study by Bouvier et al. (2005) suggested some of these ages to be secondary rather than primary.

SNC meteorites contain Martian noble-gas components derived from several major geochemical reservoirs: modern atmosphere in the shergottites, and elementally fractionated

ancient (Allan Hills [ALH] 84001) and recent (nakhlites) atmospheric components (e.g., Bogard and Johnson 1983; Becker and Pepin 1984; Ott 1988; Murty and Mohapatra 1997). At least one component derived from Martian interior is found primarily in Chassigny (Ott 1988; Mathew and Marti 2001). The isotopic composition of argon is one of the most important parameters to distinguish these components. Apart from Martian atmospheric and mantle argon, SNC meteorites contain radiogenic and inherited ^{40}Ar, cosmogenic argon (^{40}Ar/^{36}Ar << 1; ^{36}Ar/^{38}Ar ~ 0.65) and lately trapped terrestrial argon (^{40}Ar/^{36}Ar = 296; ^{36}Ar/^{38}Ar = 5.35). The multiplicity of these components makes the separation of Martian argon components problematic and various investigations have suggested diverging values of isotopic compositions for trapped argon components in Martian meteorites (e.g., Wiens 1988; Bogard and Garrison 1998; Terribilini et al. 1998; Schwenzer et al. 2007). Martian

atmospheric argon was evaluated to have a high $^{40}Ar/^{36}Ar$ ratio with an upper limit of 1900 (Bogard and Garrison 1999), or as high as 3000 ± 500 determined by the Viking mission (Owen 1992). The $^{36}Ar/^{38}Ar$ ratio associated with this high $^{40}Ar/^{36}Ar$ component was suggested to be close to 4.0 (e.g., Wiens et al. 1986; Bogard 1997), a unique value for a non-cosmogenic geochemical reservoir in the solar system, which in most cases (solar, terrestrial, or trapped Q argon) is close to a value of 5.35. This unique value seriously constrains Martian atmospheric erosion. Martian mantle argon was evaluated to have a low $^{40}Ar/^{36}Ar$ of <500 (Bogard and Garrison 1999) or even <300 (Swindle et al. 1986), hardly discernible from terrestrial atmospheric argon, and with a canonical $^{36}Ar/^{38}Ar$ ratio of 5.35. On the other hand, recent results indicate that at least some portions of the Martian interior might have argon with a $^{40}Ar/^{36}Ar$ ratio as high as the Martian atmosphere (Schwenzer et al. 2007).

Our previous high resolution ^{40}Ar-^{39}Ar stepheating studies of terrestrial and extraterrestrial plagioclase, pyroxene, and olivine mineral separates (e.g., Trieloff et al. 1997, 2003a; Korochantseva et al. 2005; Hopp and Trieloff 2005; Hopp et al. 2007) have demonstrated that neutron induced argon isotopes (besides K-derived ^{39}Ar, also Ca-derived ^{37}Ar and Cl-derived ^{38}Ar) can be used to identify and resolve radiogenic argon from various trapped argon components which can be hosted by main minerals or accessory phases. In this paper, we present comprehensive high-resolution ^{40}Ar-^{39}Ar stepwise heating analyses on whole rock and handpicked mineral separates of several Martian shergottites (Shergotty, Zagami, Sayh al Uhaymir [SaU] 005, Dhofar 019). Some non-irradiated samples (maskelynite and pyroxene of Shergotty, pyroxene of Zagami) were measured to check the contribution of interfering Cl-derived ^{38}Ar in neutron-irradiated samples. Besides the evaluation of trapped argon components, this study also intended to contribute chronological data concerning thermal history, crystallization and cratering events of the Martian lithosphere.

SAMPLE DESCRIPTIONS

Shergottites are customarily divided into three subgroups: 1) basaltic, 2) picritic or olivine-phyric/olivine-orthopyroxene-phyric, and 3) lherzolitic or peridotitic.

Dhofar 019 and SaU 005 are olivine-phyric shergottites found in hot deserts. Both meteorites contain olivine megacrysts with primary melt inclusions. In Dhofar 019, olivine megacrysts are set within a groundmass composed of finer grained olivine, pyroxene (pigeonite and augite), and maskelynite (Taylor et al. 2002). This rock experienced peak shock pressures estimated between 26–29 GPa (Fritz et al. 2005) and ≤30–35 GPa (Badjukov et al. 2001; Taylor et al. 2002). Dhofar 019 experienced extensive terrestrial weathering and its terrestrial age is 0.34 ± 0.04 Ma (Nishiizumi et al. 2002).

SaU 005 consists of olivine megacrysts set within a groundmass of low Ca-pyroxene and maskelynite (Zipfel 2000). Shock veins and up to millimeter-sized impact melt pockets are abundant (~9 vol%). Shock-melt associated vesicles are up to 3 mm in size and show a preferred orientation (Gnos et al. 2002). The meteorite is heavily shocked: >45 GPa (Gnos et al. 2002), 40–45 GPa (Fritz et al. 2005). The fresh appearance and minor terrestrial weathering products (Zipfel 2000; Gnos et al. 2002) suggest a short terrestrial age of SaU 005. Based on its ^{81}Kr-^{83}Kr apparent age, Park et al. (2003) estimated the terrestrial age of SaU 005 to be close to 0.

Zagami and Shergotty belong to "classic" basaltic shergottites whose falls were observed. Zagami is composed of up to three related basaltic lithologies and shock-melted glass veins (e.g., Meyer 2007). The Zagami lithology we used for ^{40}Ar-^{39}Ar dating is similar to Shergotty. These lithologies are relatively fine-grained and composed mostly of augite and pigeonite clinopyroxenes (≥70%) and maskelynite (≥20%). Localized melting products are observed in both meteorites (Stöffler et al. 1986; Fritz et al. 2005).

The meteorites have been severely shock metamorphosed: the equilibrium shock pressures evaluated for both Zagami and Shergotty are 29–31 GPa (Stöffler et al. 1986; Fritz et al. 2005). Meanwhile some studies indicate—at least locally—substantially higher peak shock pressures for these meteorites (e.g., Sharp et al. 1999; Langenhorst and Poirier 2000a, 2000b; Chen and El Goresy 2000; El Goresy et al. 2000, 2003).

EXPERIMENTAL TECHNIQUES

Whole rock and mineral separates were prepared by handpicking under a binocular. The samples were crushed as coarse and gently as possible: on the one hand to obtain mineral separates as pure as possible, on the other hand to avoid argon loss and incorporation of terrestrial atmospheric argon. Besides major phases such as maskelynite, pyroxene or olivine, we also separated "opaque" phases, which could comprise impact glass and/or shock metamorphosed Ca-rich augite, and/or K-rich maskelynite. Although only a very limited amount could be separated of these rare phases, we conducted analyses in order to check contributions to whole rocks. All separated material was consumed during analyses, so a detailed mineralogical characterisation of "opaque" separates was not possible.

^{40}Ar-^{39}Ar analysis followed standard procedures given by Jessberger et al. (1980) and Trieloff et al. (1994a, 1998, 2003b). Samples were wrapped in high-purity (99.999%) Al-foil and irradiated for 18.5 days in evacuated quartz ampoules, applying 1 mm cadmium shielding to suppress the $^{37}Cl(n,\gamma\beta^-)^{38}Ar$ reaction, at the GKSS-reactor in Geesthacht, Germany. Besides neutron-irradiated, some non-irradiated aliquots (pyroxene of Zagami, maskelynite and pyroxene of Shergotty) were measured to monitor Cl-derived ^{38}Ar.

The J-value was 0.80×10^{-2} as determined by 2.66 Ga old NL25 hornblende flux monitors (Schaeffer and Schaeffer 1977; Schwarz and Trieloff 2007). Correction factors for interfering isotopes determined by CaF_2 monitors were (^{36}Ar/$^{37}Ar)_{Ca} = (4.6 \pm 0.1) \times 10^{-4}$, ($^{38}Ar/^{37}Ar)_{Ca} = (8.8 \pm 0.2) \times 10^{-5}$, ($^{39}Ar/^{37}Ar)_{Ca} = (9.6 \pm 0.1) \times 10^{-4}$. ($^{38}Ar/^{39}Ar)_K = (2.3 \pm 0.23) \times 10^{-3}$ was determined via the NL25 monitors, after subtraction of Cl-induced ^{38}Ar. ($^{40}Ar/^{37}Ar)_{Ca} = (3 \pm 3) \ 10^{-3}$ was taken from Turner (1971) and ($^{40}Ar/^{39}Ar)_K = (1.23 \pm 0.24) \times 10^{-2}$ from Brereton (1970). The samples were stepwise heated to temperatures from 300 °C to 1800 °C (up to 26 temperature steps) using an induction-heated furnace with ^{40}Ar blank values of (2.7–4.2) 10^{-10} ccSTP at 850 °C and (8.1–22.0) 10^{-10} ccSTP at 1450 °C (10 min heating duration). Extraction temperatures were controlled based on heating power calibrated by a thermocouple that was damaged in the course of the analyses. While relative temperatures were reproducible to ±10 °C, absolute temperatures could have been systematically overestimated by ~100 °C. Apparent ages were calculated using the Steiger and Jäger (1977) conventions. Given uncertainties of apparent ages are 1σ.

The concentration of $^{36}Ar_{trapped}$ in most samples was calculated by component deconvolution using the $^{36}Ar/^{38}Ar$ ratios that vary between a trapped component of either 5.35 (e.g., Martian mantle) or 4.0 (Martian atmosphere) and a cosmogenic component with $^{36}Ar/^{38}Ar = 0.65$. Values lower than 0.65 indicate contributions of ^{38}Ar derived from neutron reactions on Cl during reactor irradiation. The resulting proportions of $^{36}Ar_{trapped}$ depend on the choice of the trapped endmember composition (i.e.,, 5.35 or 4.0). We analyzed the data using both endmember values and found that the difference in $^{36}Ar_{trapped}$ concentrations is only ~5%, resulting in a difference in ($^{40}Ar/^{36}Ar)_{trapped}$ ratios which is indistinguishable within 1σ errors. Hence, in text and figures we only show ($^{40}Ar/^{36}Ar)_{trapped}$ ratios and apparent ages calculated with ($^{36}Ar/^{38}Ar)_{trapped} = 5.35$. In the cases where the data indeed are distinct for ($^{36}Ar/^{38}Ar)_{trapped}$ ratios of 5.35 and 4.0, the results for both values are shown.

RESULTS AND DISCUSSIONS

^{40}Ar-^{39}Ar analytical data of studied samples are summarized in Table 1, detailed isotope data are given in the Appendix. Note that apparent ages and age spectra are usually not corrected for trapped ^{40}Ar. Only a—nominal—routine correction for primordial argon with ($^{40}Ar/^{36}Ar)_{traped} = 1 \pm 1$ is applied, which is indeed "uncorrected" within uncertainties. If further corrections for trapped excess ^{40}Ar were applied, this is explicitly stated in the text, figure captions and/or legends.

^{40}Ar-^{39}Ar Chronology
Olivine-Phyric Shergottites

Dhofar 019 and SAU 005 are desert meteorites and the low-temperature extractions of all measured samples of these meteorites contain substantial amounts of terrestrial atmospheric argon. This can be deduced from distinct low temperature release peaks of trapped ^{36}Ar, low temperature extractions defining apparent isochrons indicating trapped argon of atmospheric composition, and high apparent ages at low temperatures that in some cases exceed the age of the solar system (plots not shown here). This particularly concerns Dhofar 019, which has a long terrestrial residence time. The influence of desert weathering on argon systematics is described in detail by Korochantseva et al. (2005). The significant terrestrial contamination complicates the identification and decomposition of Martian argon components. Hence, for three isotope correlation diagrams and for the evaluation of the isotopic composition of trapped argon we excluded the contaminated low temperature extractions, and used only intermediate and high temperature extractions. In the age spectra of all Dhofar 019 and SaU 005 samples, low temperature extractions were corrected for terrestrial atmospheric argon identified in isotope correlation plots using trapped (non-cosmogenic) ^{36}Ar.

Dhofar 019

In the maskelynite separate, the release of Ca-derived ^{37}Ar and K-derived ^{39}Ar indicate degassing of maskelynite above 1000 °C (Fig. 1a). $^{36}Ar/^{38}Ar$ ratios of the various temperature extractions vary from 0.72 to 1.46, reflecting mixing of cosmogenic ($^{36}Ar/^{38}Ar = 0.65$) and trapped (e.g., atmospheric or interior) argon. For Dhofar 019 maskelynite, plotting $^{36}Ar_{trapped}/^{40}Ar_{total}$ versus $^{39}Ar/^{40}Ar_{total}$ (Fig. 2a) yields ($^{40}Ar/^{36}Ar)_{trapped}$ of 318 ± 19 for temperature extractions 930–1650°. After correction for trapped component, the age spectrum shows a well-defined plateau with an age of 642 ± 72 Ma for 9–100% ^{39}Ar release (Fig. 3c). This age is compatible with the ^{40}Ar-^{39}Ar age of ~650 Ma given for a Dhofar 019 feldspar sample measured by Garrison and Bogard (2001), and consistent with Sm-Nd and Rb-Sr ages of 575 ± 7 Ma and 525 ± 56 Ma (Borg et al. 2001; not specified if 1σ or 2σ errors), respectively.

In the pyroxene separate, most of Ca-derived ^{37}Ar and K-derived ^{39}Ar are released above 1000 °C. However, K-derived ^{39}Ar degasses similar as from maskelynite (maximum release at 1340 °C, Table A3, cf. Fig. 1), while ^{37}Ar degasses differently (maximum release at 1480 °C, Table A3), similar to other pyroxene separates (Trieloff et al. 1997, 2003a; Korochantseva et al. 2005). A comparison of the K concentration of the pyroxene separate computed from K-derived ^{39}Ar (328 ppm) (Table 2) with the K content of pyroxene mineral grains measured by electron microprobe analyses (EMPA—Taylor et al. 2002)—generally below the detection limit—demonstrates that most ^{39}Ar degasses not from pyroxene mineral grains, but from K-bearing impurities. This is most likely maskelynite, as judged from degassing temperature and the observation that other K bearing phases like melt inclusions were not reported for Dho 019 pyroxene (only olivine, see below; Taylor et al. 2002). Accordingly,

Table 1. Summary results from Ar-Ar dating of shergottites. Argon concentrations are given in units of 10^{-8} ccmSTP/g, production rates used for calculations of CRE ages in units of 10^{-10} ccmSTP/[g Ma Ca]. Errors are 1σ.

Meteorite	Sample	$^{38}Ar_{sp}$	$^{38}Ar_{tr}$	$^{38}Ar_{Cl}$	$(^{40}Ar/^{36}Ar)_{tr}$	Ar-Ar age (Ma)	Production rate	CRE age (Ma)
Dhofar 019	Maskelynite	2.443(2.248)*	2.081(2.276)		318 ± 19 (303 ± 18)	642 ± 72	2.00	15.8 ± 1.0
	Pyroxene	2.158(1.992)	1.109(1.275)		370 ± 18 (352 ± 16)	603 ± 96	2.03	(15.6 ± 1.0)
	Olivine	1.125(0.931)	1.879(2.073)		341 ± 73 (325 ± 70)	1086 ± 252		
	Opaque	9.10(4.66)	119.61(124.04)					
	Whole rock	1.831(1.790)	0.191(0.233)		1/296	$1044 \pm 35/948 \pm 100$		
SaU 005	Glass	0.182(0.091)	0.254(0.344)		~1200		2.35**	~1.6 (~1.0)
	Olivine	0.262(0.236)	0.064(0.090)		297 ± 20 (284 ± 19)	885 ± 66		
	Pyroxene	0.752(0.182)	3.218(3.788)					
	Maskelynite	0.660(0.313)	0.980(1.327)		296	<830	1.84	≥ 1.4 (≥ 1.0)
	Whole rock	0.248(0.243)	0.012(0.017)	0.022	1/296	$736 \pm 29/713 \pm 35$	2.27	~1.0–1.4
Shergotty	Maskelynite	0.680(0.675)	0.013(0.019)	0.087	~1200***	~370	1.93	>4
	Pyroxene	0.373(0.352)	0.053(0.074)	0.004	~1540 (~1460)	~420	2.07	2.1–2.5
	Glass	1.545(1.250)	0.732(1.027)		1812 ± 36 (1727 ± 36)		2.44	>8 (>6)
	Whole rock	0.568(0.553)	0.054(0.069)	0.368	1 / 296	391 ± 11 / K/Ar age: ~400	2.14	>2.5 (>2.4)
	Px-nonir	0.377(0.347)	0.080(0.110)					
	Mask-nonir	0.273(0.263)	0.026(0.037)					
Zagami	Maskelynite	0.518(0.516)	0.003(0.004)	0.280			1.91	>4.5
	Pyroxene	0.496(0.490)	0.021(0.029)	0.076			2.05	2.2–2.5
	Opaque	1.243(0.890)	1.647(2.000)					
	Whole rock	0.591(0.579)	0.033(0.046)	0.303			2.09	2.4–3.0
	Px-nonir	0.416(0.381)	0.091(0.126)					

*Values for cosmogenic argon in brackets were calculated using $(^{36}Ar/^{38}Ar)_{trapped} = 4.0$.
**Calculated using glass chemical compositions close to the bulk-rock composition from Gnos et al. (2002) as for ^{40}Ar-^{39}Ar dating big grains of glass were preferentially picked.
***Calculated using $(^{36}Ar/^{37}Ar)_{min}$.

maskelynite dominates the age information. The $^{36}Ar/^{38}Ar$ ratios of the various temperature extractions range from 0.72 to 1.76. In the three-isotope correlation diagram (Fig. 2b) the temperature extractions 950–1340 °C yield intercept for the $(^{40}Ar/^{36}Ar)_{trapped}$ ratio of 370 ± 18. After correction for trapped component, the age spectrum of the pyroxene separate displays a plateau over 60% of the ^{39}Ar release with an age value similar to the maskelynite separate (Fig. 3d).

The argon release patterns of the olivine megacryst separate (not shown, but see appendix tables) indicate that the major part of all argon isotopes (including K-derived ^{39}Ar and Ca-derived ^{37}Ar) is released below 1600 °C. As olivine is characterised by release temperatures of 1600 °C (Hopp and Trieloff 2005) most argon is not released from (K- and Ca-poor) olivine, but from additional K and Ca bearing phases. Since most olivine megacrysts contain inclusions consisting mainly of a glass and augite (Taylor et al. 2002), we conclude that predominantly these inclusions control the release and the age spectra. $^{36}Ar/^{38}Ar$ ratios of the temperature extractions are between 0.93 and 1.58. The temperature extractions 950–1550 °C contain trapped argon with a $(^{40}Ar/^{36}Ar)_{trapped}$ ratio of 341 ± 73. Corrected for the trapped component, the ^{40}Ar-^{39}Ar age spectrum displays an age plateau of 1086 ± 252 Ma for 26–81% of the ^{39}Ar release (Fig. 3e).

We also separated "opaque" phases, possible shock metamorphosed Ca-rich augite and K-rich maskelynite and impact glass, however, their exact identification is uncertain. This separate has the highest ^{39}Ar and ^{37}Ar concentrations among the Dhofar 019 samples and has ^{36}Ar, ^{38}Ar and ^{40}Ar concentrations by 5–22 times more than those of maskelynite (excluding the low temperature fractions). The $^{36}Ar/^{38}Ar$ ratios range from 1.5 to 4 suggesting a high proportion of trapped argon. The $^{40}Ar/(^{36}Ar)_{trapped}$ ratio of temperature fractions 1050–1450 °C are low, ~300–350. The high apparent ages of these fractions (>4 Ga) imply a large ratio of excess ^{40}Ar relative to in situ radiogenic ^{40}Ar.

In Dhofar 019 whole rock sample, the $^{36}Ar/^{38}Ar$ ratios are between 0.65 and 1.4, indicating similar proportions of cosmogenic and trapped argon as in the mineral separates. In the isotope correlation plot of $^{36}Ar_{trapped}/^{40}Ar_{total}$ versus $^{39}Ar/^{40}Ar$ (not shown here), the extractions below 1200 °C and above 1400 °C yield an intercept similar to terrestrial atmospheric argon, while the 1200–1400 °C extractions contain negligible amounts of trapped ^{36}Ar. The age spectrum (Fig. 3f) corrected with air-like argon composition has still an irregular shape. Apparent ages decrease stepwise towards the end of the spectrum. In a multimineralic whole rock sample this could be ascribed to ^{39}Ar recoil redistribution, e.g., implantation from K-rich glass into K-poor, retentive olivine (Turner and Cadogan 1974; Huneke and Smith 1976). Six intermediate extractions (1200–1400 °C) show a fairly constant age over ~20–78% of the ^{39}Ar release with an average age of 948 ± 100 Ma [using $(^{40}Ar/^{36}Ar)_{trapped}$ = 296 and $(^{36}Ar/^{38}Ar)_{trapped}$ = 5.35] and 1044 ± 35 Ma [if $(^{40}Ar/$
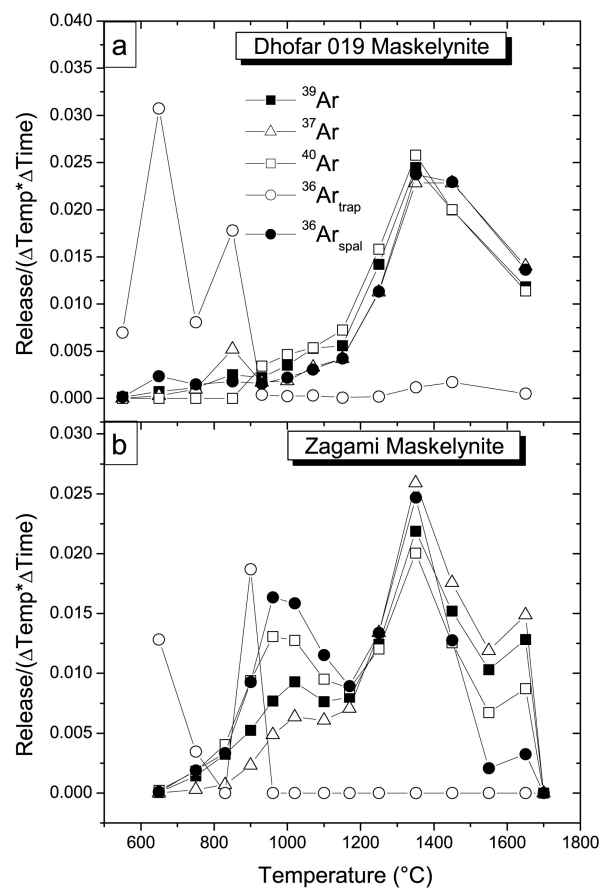

Fig. 1. Release patterns of argon isotopes of maskelynites. a) Dhofar 019 and b) Zagami.

$^{36}Ar)_{trapped}$ = 1 and $(^{36}Ar/^{38}Ar)_{trapped}$ = 5.35] (Fig. 3f). These values appear significantly higher than the maskelynite age, which should dominate the age of the whole rock sample, as it is abundant (~26 vol%) and the main K-bearing mineral phase (Taylor et al. 2002). Garrison and Bogard (2001) also found that Dhofar 019 whole rock appears to have a higher age than maskelynite (Table 3). The discrepancy can be caused by the inappropriate correction of the intermediate temperature extractions of the whole rock sample, which may contain trapped argon with $(^{40}Ar/^{36}Ar)_{trapped}$ significantly higher than 296. Such argon is detected in pyroxene and olivine separates, which indeed should contribute to the whole rock sample noticeably. These considerations underline the necessity to measure multiple mineral separates of a rock, as deconvolution from a whole rock sample alone may be impossible due to interference of multiple components.

Dho 019 Summary

Our best age estimate of Dho 019 is given by the maskelynite age of 642 ± 72 Ma. This age is consistent with the value of ~650 Ma obtained by Garrison and Bogard (2001), and agrees with Sm-Nd and Rb-Sr ages of 575 ± 7 Ma and 525 ± 56 Ma measured by Borg et al. (2001) (Table 3).
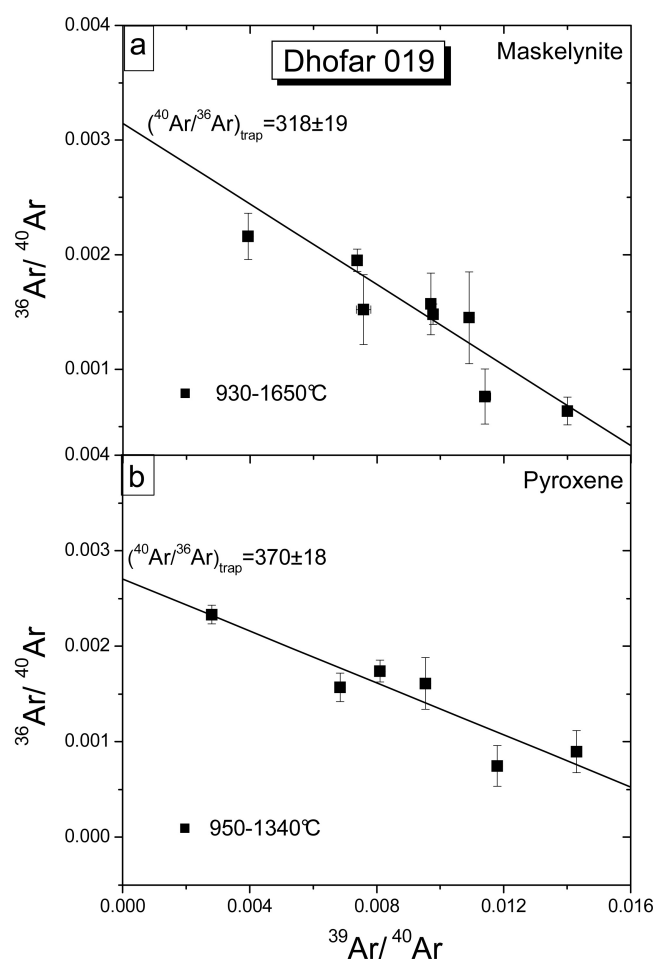
Fig. 2. Three isotope correlation diagrams $^{36}Ar_{trap}/^{40}Ar$ versus $^{39}Ar/$ ^{40}Ar ratios for Dhofar 019 maskelynite (a) and pyroxene (b) constrain the composition of trapped Ar of intermediate and high temperature extractions.

The age of glass inclusions within olivine (1086 ± 252 Ma) could date the entrapment of magmatic liquid during crystallization, while the maskelynite age implies later appearance of plagioclase in this mineral assemblage. Such a scenario was envisaged by Taylor et al. (2002) who presented evidence that some of the olivine grains may be of cumulate origin, i.e., genetically unrelated megacrysts crystallised significantly earlier. Alternatively, excess ages of glass inclusions could simply reflect the presence of magmatic argon with a highly radiogenic signature. The higher age of the melt-inclusions within olivines compared to maskelynite could be also caused by late reset or cooling. In this case Rb-Sr and Sm-Nd systems should have been affected as well, while glass inclusions may have been protected against reset by the highly retentive olivine crystals. However, slow cooling seems unlikely regarding the thermal history of Dhofar 019 deduced from petrographic observations (Taylor et al. 2002; see also section Young or Old Shergottites?). Concluding, the most likely explanation of the apparently

high glass inclusion age of 1086 ± 252 Ma seems to us entrapment of magmatic argon with a radiogenic signature upon formation ~600 Ma ago.

Sayh al Uhaymir 005

The SaU 005 glass separate comprises shock veins and up to millimeter-sized impact melt pockets, which have an abundance of ~9 vol% (Zipfel 2000). The separate contains significant amounts of trapped argon, which is reflected, e.g., by relatively high $^{36}Ar/^{38}Ar$ ratios of individual temperature extractions between 2.3 and 3.9. This sample shows a distinct release peak of all argon isotopes at ~1380 °C (Appendix Table A7) and has a saddle shaped age spectrum with high apparent ages generally >3 Ga (Fig. 4c). The temperature extractions above 1380 °C display apparent ages exceeding the age of the solar system that is indicative of the presence of excess argon. Correction for a terrestrial air-like trapped component (indicated by low temperature steps in Fig. 5a) results in an age spectrum with stepwise increasing apparent ages between 1 and 5 Ga (Fig. 4c), i.e., unrealistically high apparent ages caused by excess argon are not removed. The $^{40}Ar_{total}/^{36}Ar_{trapped}$ ratios of 900–1190 °C fractions are 500–800. As seen from a three isotope correlation diagram (Fig. 5a), the extractions of 1220–1460 °C form an almost horizontal array with a constant $^{40}Ar_{total}/^{36}Ar_{trapped}$ ratio of ~1200. Stepwise increasing ages in the age spectrum can possibly be explained by diffusional loss of previously trapped Martian atmospheric argon during a thermal event: If a high $^{40}Ar_{total}/$ $^{36}Ar_{trapped}$ component was better retained in highly retentive phases, this would cause particularly high apparent excess ages at high temperature extractions. Such an explanation is consistent with the suggestion of Schwenzer et al. (2002) that SaU 005 glass originally had a much higher concentration of trapped Martian gases primarily retained in vesicles, which were lost during strong recrystallisation. Correction of the high temperature fractions with a $(^{40}Ar/^{36}Ar)_{trapped}$ ratio of 1200 decreases apparent ages below 3 Ga, but with very high uncertainties.

In the olivine megacrysts, the $^{36}Ar/^{38}Ar$ ratios range from 1.22 to 1.99. In the isochron plot (Fig. 5b), 1200–1780 °C extractions form distinct array with intercept of $(^{40}Ar/$ $^{36}Ar)_{trapped}$ ratio of 297 ± 20. After correction, the olivine age spectrum (Fig. 4d) displays a plateau of 885 ± 66 Ma, comprising three extractions with 83% of the total ^{39}Ar release. Release patterns of neutron induced argon isotopes and the comparison of Ca and K concentrations obtained by EMPA and ^{40}Ar-^{39}Ar analyses indicate that the primary melt inclusions— which are common in olivine (Gnos et al. 2002)— probably dominate the age information. The first two extractions of 800 and 1000 °C show a separate release peak of $^{36}Ar_{trapped}$ and ^{40}Ar and maintain high apparent ages after correction of the age for trapped argon. Assuming the 885 Ma age is a valid date, these extractions suggest a $(^{40}Ar/^{36}Ar)_{trapped}$ ratio of ~400.
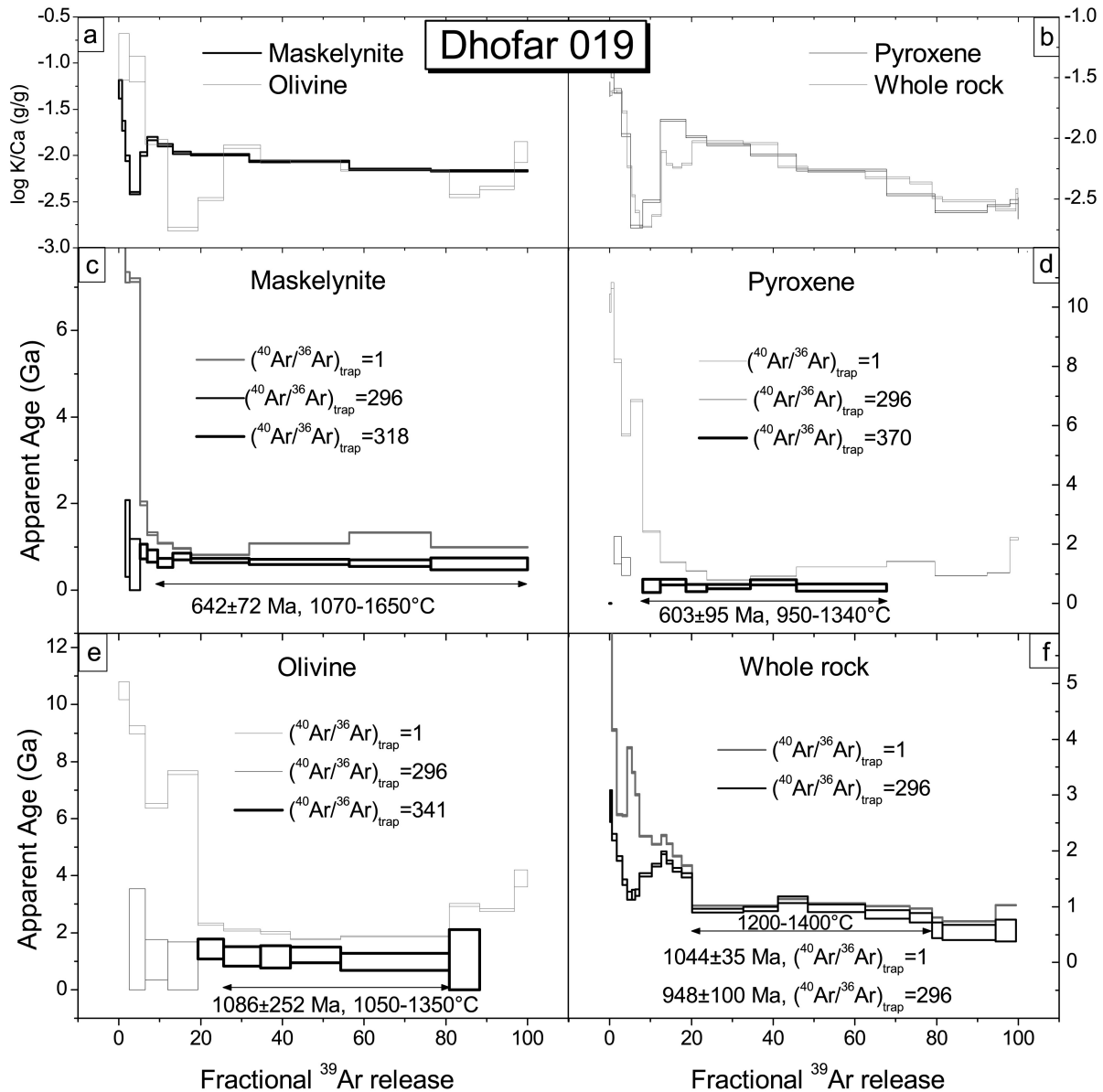
Fig. 3. K/Ca spectra (a, b) and age spectra (c–f) of Dhofar 019 samples before and after correction for trapped components (note that the "uncorrected" age spectrum contains a nominal routine correction for primordial argon with $(^{40}Ar/^{36}Ar)_{trap} = 1 \pm 1$, i.e., uncorrected within uncertainties). For mineral separates of Dhofar 019, the compositions of trapped components were identified by the three isotope correlation plots. For Dhofar 019 whole rock, air-like argon composition was tentatively applied to correct all temperature steps.

In the pyroxene separate, the $^{36}Ar/^{38}Ar$ ratios are 2.8–4.8, again indicating substantial proportions of trapped argon. The presence of excess argon is seen also from the age spectrum, which displays apparent ages >3.7 Ga (Fig. 4e), if corrected for $(^{40}Ar/^{36}Ar)_{trapped} = 1$. From the three isotope plot (not shown here), $(^{40}Ar/^{36}Ar)_{trapped}$ ratio of ~300 is inferred. Correction with this component results in high uncertainties in apparent ages, precluding chronological evaluation (Fig. 4e). Melt inclusions (Gnos et al. 2002) and/or maskelynite impurities are also present in pyroxene grains and obviously dominate the measured K budget of the pyroxene separate, similar to primary melt inclusions in olivine.

The $^{36}Ar/^{38}Ar$ ratios in the maskelynite separate are >1.3. As revealed by the three isotope correlation diagram, the data of 600–1400 °C fractions form a trend yielding an intercept of a terrestrial atmosphere-like $^{36}Ar/^{40}Ar$ ratio. However, this trend includes the low temperature extraction(s) contaminated by terrestrial atmospheric argon. Both the low resolution of this analysis and the atmospheric contamination make it difficult to constrain the proper composition of the extraterrestrial trapped component. If corrected for an air-like trapped component, two major fractions with 66% of the total ^{39}Ar release have apparent ages <830 Ma (Fig. 4f).

The $^{36}Ar/^{38}Ar$ ratios of extractions from the whole rock

Table 2. Ca and K concentrations of measured samples inferred from K-derived ^{39}Ar and Ca-derived ^{37}Ar and obtained by standard methods (K_M and Ca_M).

Meteorite	Sample	K_{Ar-Ar} (%)	K_M (%)	Ca_{Ar-Ar} (%)	Ca_M (%)
Dhofar 019[a]	Maskelynite	0.0634 ± 0.0023	0.12[*]	7.876 ± 0.330	9.57[*]
	Pyroxene	0.0328 ± 0.0015	<0.02[**]	7.283 ± 0.478	7.33
	Olivine	0.0185 ± 0.0009	<0.02[**]	3.355 ± 0.158	0.21
	Opaque	0.1257 ± 0.0082		10.645 ± 1.594	
	Whole rock	0.0288 ± 0.0007	0.04	6.245 ± 0.195	6.62
SaU 005[b]	Glass	0.0087 ± 0.0002	n.a.	2.682 ± 0.094	3.21
	Olivine	0.0161 ± 0.0005	b.d.	4.891 ± 0.181	0.21–0.63
	Pyroxene	0.0295 ± 0.0042	b.d.–0.03	5.048 ± 0.636	2.49–4.92[***]
	Maskelynite	0.0514 ± 0.0058	0.05–0.12	8.774 ± 1.667	8.09–9.39
	Whole rock	0.0169 ± 0.0005	0.02	4.257 ± 0.189	4.10
Shergotty	Maskelynite	0.3052 ± 0.0397	0.27[c];0.344[d]	6.94 ± 1.278	7.18[c]
	Pyroxene	0.0202 ± 0.0005	0.0175[d]	5.791 ± 0.522	7.32[c]
	Glass	0.1815 ± 0.0026	0.23[c]	6.047 ± 0.129	6.42[c]
	Whole rock	0.1595 ± 0.0015	0.14[e];0.181[d]	6.232 ± 0.121	6.86[e]
Zagami	Maskelynite	0.3012 ± 0.0166	0.24[c]	6.236 ± 0.405	7.64[c]
	Pyroxene	0.0413 ± 0.0012	0.0435[f]	8.607 ± 1.767	8.03[c]
	Opaque	0.084 ± 0.0018		4.448 ± 0.126	
	Whole rock	0.1674 ± 0.0027	0.12[e]	7.977 ± 0.181	7.50[e]

[a]Taylor et al. (2002); [b]data of whole rock by Dreibus et al. (2000) and of mineral phases by Gnos et al. (2002) analyzed shergottite SaU 094, which is considered to be paired with SaU 005; [c]Stöffler et al. (1986); [d]Terribilini et al. (1998); [e]Lodders (1998); [f]Shih et al. (1982).

[*]Data of Ca-rich maskelynite representing the largest grains which were preferably picked for ^{40}Ar-^{39}Ar dating.

[**]Equivalent to below detection limit.

[***]Range of pigeonite analyses as augite occurs rarely.

Abbreviations: b.d. = below detection limit; n.a. = not analyzed.

sample are mostly lower than the cosmogenic value, in particular in the temperature range of 900–1280 °C. Such low values are attributed to the interference of Cl-derived ^{38}Ar, and preclude a reasonable evaluation of the $(^{40}Ar/^{36}Ar)_{trapped}$ ratios. Hence, we cannot correct for a possible excess argon component and the following values are upper limits. The flattest part, the nine extractions 1040–1400 °C releasing 71% of the ^{39}Ar release (Fig. 6) give an average age of 736 ± 29 Ma and 713 ± 35 Ma, if corrected with $(^{40}Ar/^{36}Ar)_{trapped} = 1$ and $(^{40}Ar/^{36}Ar)_{trapped} = 296$, respectively.

SaU 005 Summary

The obtained ^{40}Ar-^{39}Ar ages of SaU 005 samples range between 700–900 Ma and do not agree with a recently estimated Sm-Nd age of 445 ± 18 Ma interpreted as an igneous event (Shih et al. 2007). This could be due to an improper correction for trapped argon. The evaluation of the latter may be either hampered by Cl-produced ^{38}Ar, or by the presence of various trapped argon components with largely differing $(^{40}Ar/^{36}Ar)_{trapped}$ ratios between 300 and 1200. By analogy with Dhofar 019 Martian meteorite we could expect a coincidence of the Sm-Nd age with the maskelynite ^{40}Ar-^{39}Ar age which is, however, poorly constrained yet. It is worth to note that SaU 005 experienced not only strong shock effects, but also a thermal event that caused recrystallization of glass (see Schwenzer et al. 2002) and olivine (Gnos et al. 2002) as well as equilibration of mineral compositions observed for this meteorite (Gnos et al. 2002). Indeed, high-

temperature SaU 005 glass indicates diffusional loss of argon. Hence, the above-mentioned Sm-Nd age could date the secondary event rather than a primary one (see section Young or Old Shergottites?). Jagoutz et al. (2006) report that Sm-Nd and Rb-Sr isotopic systems of olivine shergottites (e.g., SaU 005, DaG 476, Y-980459) are highly disturbed. Analysing the existing data they favor an age of 800 Ma for the olivine shergottites, consistent with the age of the olivine separate. This age may be interpreted as the crystallization age if glass inclusions within the highly retentive olivine crystals were not affected by secondary event(s). Earlier estimated K-Ar ages of SaU 005 whole rock samples are ~1000 Ma (assuming all ^{40}Ar is radiogenic) and ~870 Ma, assuming all trapped ^{36}Ar is due to terrestrial atmospheric contamination (Pätsch et al. 2000).

Basaltic Shergottites

Shergotty

With the exception of the first extraction, the ^{36}Ar/^{38}Ar ratios of the maskelynite separate vary from 0.48 to 0.96. ^{36}Ar/^{38}Ar ratios below the cosmogenic production ratio of 0.65 indicates significant contributions of Cl-derived ^{38}Ar produced during neutron irradiation, released from Cl-bearing phases like apatite (here we also note that even in the case of ^{36}Ar/^{38}Ar > 0.65, Cl-contributions cannot be excluded, though not proven). The presence of Cl-derived ^{38}Ar allows conventional quantification of $^{36}Ar_{trapped}$ in only a

Table 3. Literature data of radiometric and cosmic ray exposure (CRE) ages. All ages are given in Ma.

	Dhofar 019	SaU 005	Shergotty	Zagami
Radiometric ages				
Ar-Ar	~650 (mask), ~780–620 (wr)[a]		254 ± 10 (mask), 240–640 (wr)[i]; 167–195[j]	223 ± 6 (mask)[u,***]; 209 ± 2 (mask)[i,u,****]; ~260 (mask)[v]
K-Ar	750–1430[b]; 540 ± 20[c]	1010–1510[b]; ~870–1000[f]	387[j]; 196 ± 40[k]; ~130[l]; 560^{+60}_{-150}[m]	242[i]; ~150[l]
Rb-Sr	525 ± 56[d]		165 ± 11[n]; 167 and 360[o]	166 ± 12, 177 ± 9, 166 ± 6, 178 ± 4[w]: 180 ± 4[v], 186 ± 5 and 183 ± 6[x]; 184 ± 8 and 183 ± 12[p]
Sm-Nd	575 ± 7[d]	445 ± 18[g]	147 ± 20 and 360 ± 16[o]; 620 ± 170[p]	180 ± 37[x]; 155 ± 9[y]
U, Th-Pb			200 ± 4, 205 ± 8, 600 ± 20, 437 ± 36[q]; 217 ± 110 and 189 ± 83[r]	230 ± 5, 229 ± 8[q]; 163 ± 4[z]
Pb-Pb				4048 ± 17[y]
Lu-Hf				185 ± 36[y]
CRE ages				
^{3}He	11.1–14.4[b,c]	0.86–1.27[b,h]	2.0–3.3[l,s]	2.1–3.7b[l,s]
^{21}Ne	17.0–23.7[b,c]	0.75–0.83[b,h]	3.2–4.0[l,s]	2.1–4.18b[l,s]
^{38}Ar	14.5–14.9[b]; 20.1–22.6[c,*]	0.81–1.06[b,h]	1.97–3.0[l,s]	1.9–2.6b[l,s]
^{83}Kr			1.67[l]	2.17[l]
^{126}Xe			4.40[l]	3.67[l]
^{81}Kr-^{83}Kr	20.4[b]	0.81[b]	3.05 ± 0.50[h]	2.98 ± 0.3[h]
Average	19.6 0.4 (T_{21-38})[c,*]	1.5 ± 0.3 (T_{3-38})[f]; 0.89 ± 0.15 (T_{3-38})[h]; 1.2 ± 0.3[h,**]	2.66 (T_{3-38}), 2.85 (T_{3-126})[l]; 2.9 ± 0.4 (T_{3-38})[k]; 3.1 ± 0.4 (px,T_{3-38})[k]; 2.73 ± 0.20[**]; 3.0 ± 0.3[h,**]	2.77 (T_{3-38}), 2.85 (T_{3-126})[l]; 2.92 ± 0.15[l,**]; 3.0 ± 0.2[h,**]

[a]Garrison and Bogard (2001); [b]Park et al. (2003); [c]Shukolyukov et al. (2002); [d]Borg et al. (2001); [e]Nishizumi et al. (2002); [f]Pätsch et al. (2000); [g]Shih et al. (2007); [h]Eugster et al. (2002); [i]Bogard et al. (1979); [j]Bogard and Garrison (1999); [k]Terribilini et al. (1998); [l]Schwenzer et al. (2007); [m]Geiss and Hess (1958); [n]Nyquist et al. (1979a); [o]Jagoutz and Wänke (1986); [p]Nyquist et al. (1979b); [q]Chen and Wasserburg (1986); [r]Sano et al. (2000); [s]data compiled by Terribilini et al. (2000); [t]Nyquist et al. (2001); [u]Bogard and Park (2007a), [v]Shih et al. (1982); [w]Nyquist et al. (2006); [x]Nyquist et al. (1995); [y]Bouvier et al. (2005); [z]Borg et al. (2003).

*Incorrect production rate used for ^{38}Ar$_{cosm}$.
**Compiled preferred CRE age.
***^{36}Ar corrected for cosmogenic argon.
****^{36}Ar not corrected for cosmogenic argon.
*****^{36}Ar not corrected for cosmogenic argon.

Abbreviations: T_{21-38} = average age from cosmogenic ^{21}Ne and ^{38}Ar; T_{3-38} = average age from cosmogenic ^{3}He, ^{21}Ne, ^{38}Ar; T_{3-126} = average age from cosmogenic ^{3}He, ^{21}Ne, ^{38}Ar, ^{83}Kr, ^{126}Xe; wr = whole rock; mask = maskelynite; px = pyroxene.

Most errors were specified as 2σ (Terribilini et al. [1998]; Bogard and Garrison [1999]; Sano et al. [2000]; Eugster et al. [2002]; Bouvier et al. [2005], other studies did not specify if 1σ or 2σ errors are given (Chen and Wasserburg [1986]; Jagoutz and Wänke [1986]; Borg et al. [2001]; Bogard and Park [2007a]; Shih et al. [2007]), although the use of 2σ errors is more common.
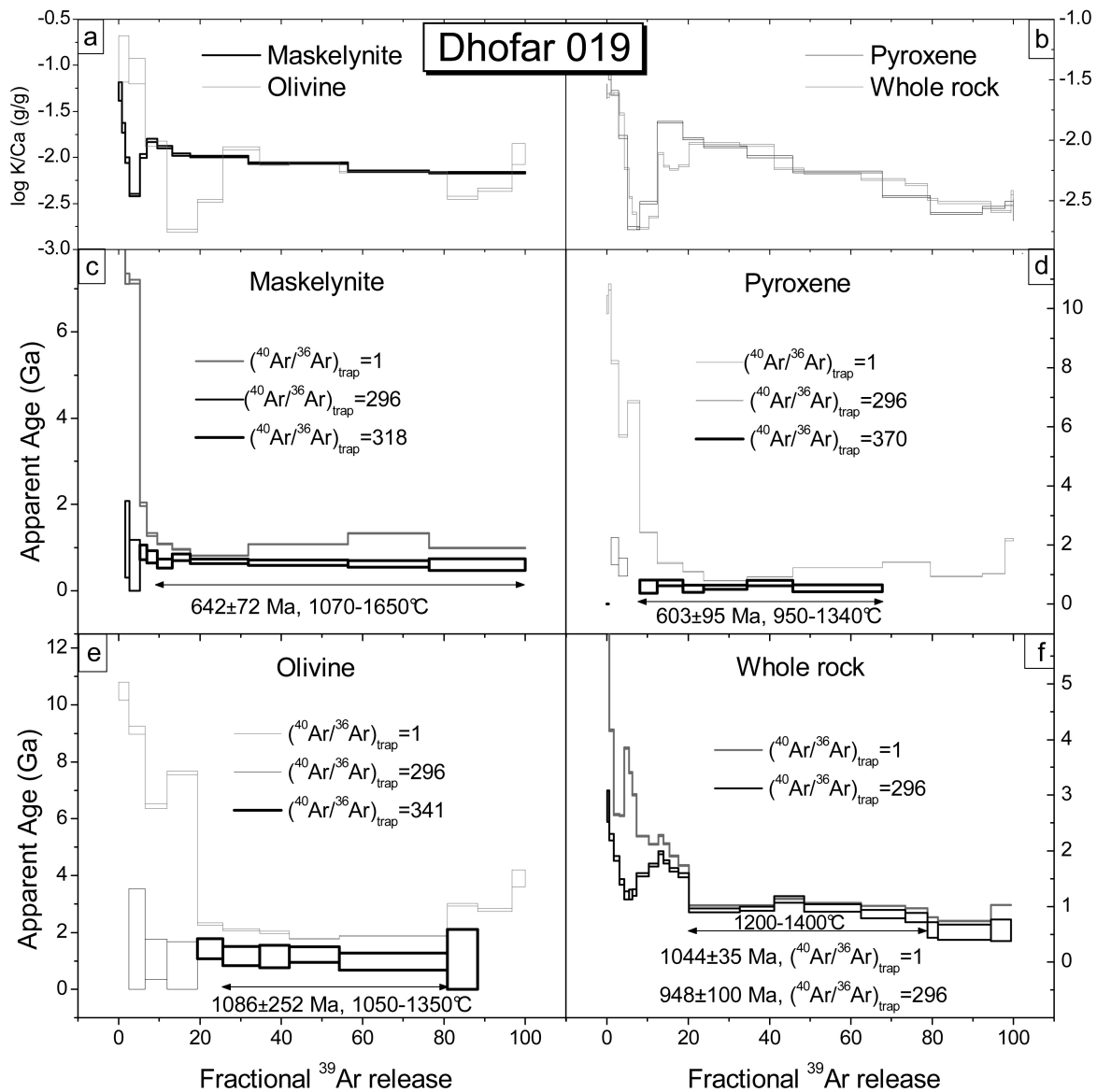
Fig. 4. K/Ca spectra (a, b) and age spectra (c–f) of SaU 005 mineral separates.

few extractions, e.g., recognition of a distinct peak of $^{36}Ar_{trapped}$ at ~900 °C, at the onset of maskelynite degassing between 800 °C and 1700 °C. In case of severe Cl-induced ^{38}Ar interference another approach described by Bogard and Garrison (1999) can be used to disentangle $^{36}Ar_{trapped}$ and $^{36}Ar_{cosmogenic}$: the minimum $^{36}Ar/^{37}Ar$ ratio (0.002 at 1250 °C) is considered as upper limit for the ratio of cosmogenic ^{36}Ar (produced mainly from Ca) and Ca-derived ^{37}Ar in individual temperature steps. However, it should be kept in mind that there are limitations of this method: cosmogenic argon is also produced by other target elements than Ca, e.g., Fe or K, and these target elements can be concentrated in different phases (e.g., Fe in metal or olivine, or K in feldspar of a whole rock sample). These can release cosmogenic ^{36}Ar quite differently, leading to unrecognized contributions of cosmogenic ^{36}Ar in

some extractions. Yet this limitation does not apply to mineral separates in which cosmogenic ^{36}Ar from different target elements is degassing from the same mineral (e.g., from Fe and Ca in pyroxene, or from K and Ca in feldspar). In the isotope correlation plot of $^{36}Ar_{trapped}/^{40}Ar_{total}$ versus $^{39}Ar/^{40}Ar_{total}$ (Fig. 7), the data of temperature extractions 650–1350 °C follow a mixing line between trapped $^{40}Ar/^{36}Ar$ ~1200 and a $^{39}Ar/^{40}Ar$ intercept corresponding to a ^{40}Ar-^{39}Ar age of ~370 Ma. This is higher than the previously reported ^{40}Ar-^{39}Ar age of Shergotty maskelynite 254 ± 10 Ma (Table 3; Bogard et al. 1979). A correction of the age spectrum with $^{36}Ar_{trapped}$ derived from component deconvolution using the $^{36}Ar/^{38}Ar$ ratios is insufficient due to underestimation of $^{36}Ar_{trapped}$: the apparent ages decrease with extraction temperature, and the extractions corresponding to the peak of
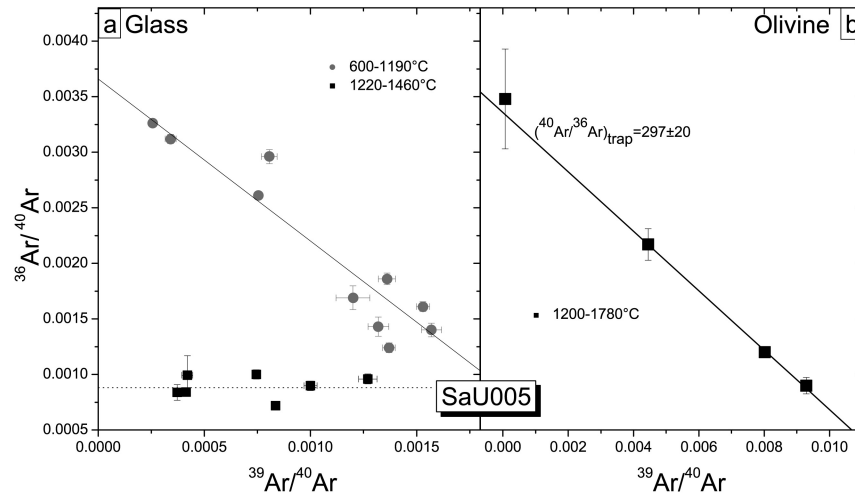
Fig. 5. Isochron plots of $^{36}Ar_{trap}/^{40}Ar$ versus $^{39}Ar/^{40}Ar$ ratios for SaU 005 glass (a) and olivine (b). The horizontal array with a constant $^{40}Ar/$ $^{36}Ar_{trap}$ ratio (~1200) for 1220–1460 °C extractions of SaU 005 glass could be caused by the diffusional loss of argon during a thermal event.
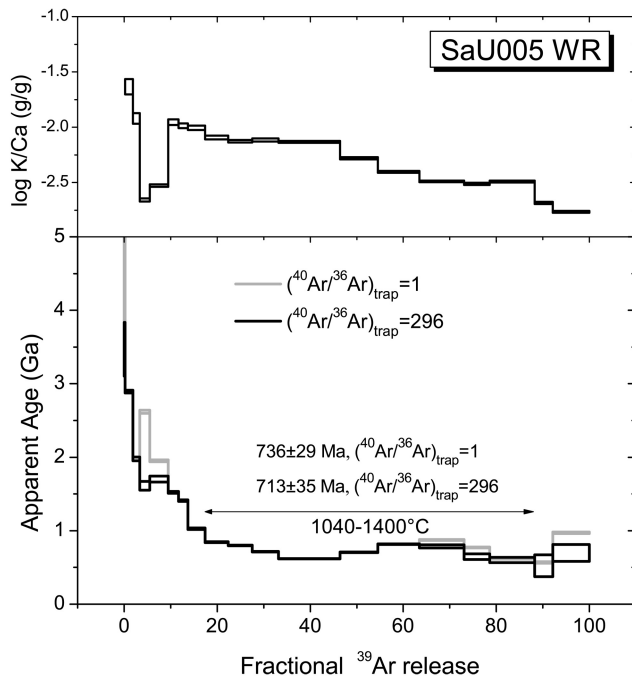

Fig. 6. K/Ca and age spectra of SaU 005 whole rock. The presence of excess argon likely influences the shape of this age spectrum.

maskelynite degassing show constant ages of about 400 Ma for 39–93% of the ^{39}Ar release (Fig. 8).

In the pyroxene separate, the $^{36}Ar/^{38}Ar$ ratios of the extractions 850–1650 °C vary between 0.94 and 2.3. The release curve of Ca-derived ^{37}Ar indicates degassing of pyroxene at 1200–1600 °C (Fig. 9a). The ^{39}Ar release peak at 700–1000 °C is very probably related to K-bearing melt inclusions in the pyroxenes, which are an important assemblage in Shergotty (e.g., Nyquist et al. 1979a). At similar temperatures of 800–1100 °C, there is a release peak of trapped ^{36}Ar with high $^{40}Ar_{total}/^{36}Ar_{trapped}$ ratios. The ($^{40}Ar/$

$^{36}Ar)_{trapped}$ ratio of this component is ~1540, as revealed by a mixing line in the three isotope correlation diagram (Fig. 7). This mixing line indicates a radiogenic component with an age of ~420 Ma. Significant amounts of $^{36}Ar_{trapped}$ are released at higher temperatures corresponding to pyroxene degassing, but the $^{40}Ar_{total}/^{36}Ar_{trapped}$ ratios of 400–500 are low. The uncorrected age spectrum shows stepwise increasing apparent ages (Fig. 10a). A correction of the high temperature fractions for an air-like trapped component does hardly remove this basic pattern and suggests the presence of excess or inherited ^{40}Ar.

The $^{36}Ar/^{38}Ar$ ratios of the glass separate extractions vary from 1.2 to 2.4. The release patterns of this sample show peaks of ^{37}Ar, ^{39}Ar, ^{40}Ar, and $^{36}Ar_{trapped}$ at ~1450 °C. The extractions 850–1450 °C contain trapped argon with $^{40}Ar/$ ^{36}Ar ratio of 1812 ± 36. Correction for the evaluated trapped component significantly decreases the high apparent ages of the uncorrected age spectrum (Fig. 10b).

In the whole rock sample, the $^{36}Ar/^{38}Ar$ ratio of 650–1350 °C extractions is from 0.15 to 0.63, suggesting considerable amounts of Cl-derived ^{38}Ar, which precludes proper quantification of trapped ^{36}Ar at intermediate temperature steps. The high temperature extractions (>1400 °C) degas minor amounts of trapped ^{36}Ar with low $^{40}Ar_{total}/^{36}Ar_{trapped}$ ratios <600. The $^{40}Ar_{total}/^{36}Ar_{trapped}$ ratios of the low temperature fractions are ~250–300. The age spectrum appears saddle shaped, but relatively flat in the intermediate part (Fig. 8), and is very similar to previous measurements by Bogard and Garrison (1999). We calculated an average age of 391 ± 11 Ma for extractions degassing over 22–75% ^{39}Ar release. Assuming the presence of air-like trapped argon in some extractions, the K/Ar age of the whole rock sample is ~400 Ma (Table 1). The total ^{40}Ar-^{39}Ar age obtained by Bogard and Garrison (1999) is 387 Ma (Table 3).
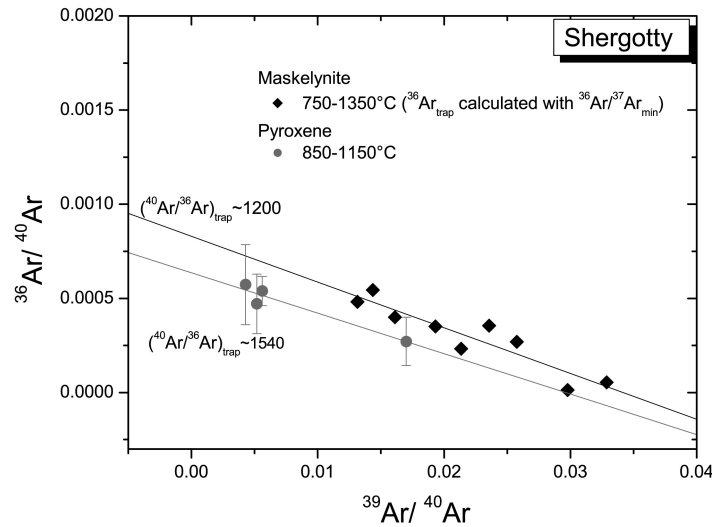
Fig. 7. Three isotope correlation diagram $^{36}Ar_{trap}/^{40}Ar$ versus $^{39}Ar/^{40}Ar$ ratios for Shergotty maskelynite (a) and pyroxene (b). For maskelynite, $^{36}Ar_{trap}$ is derived from component deconvolution assuming the minimum $^{36}Ar/^{37}Ar$ ratio of 0.002 at 1250 °C as cosmogenic argon.
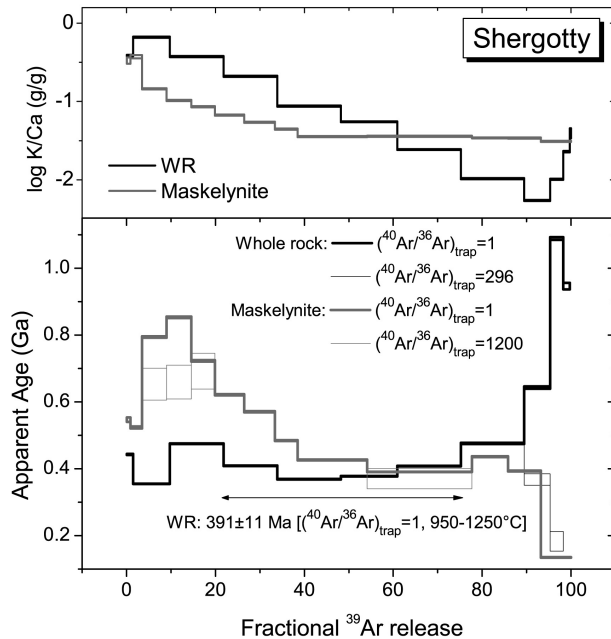

Fig. 8. K/Ca and age spectra of Shergotty maskelynite and whole rock.

Shergotty Summary

There are considerable variations in Ar-Ar age data for Shergotty from the literature (Table 3), similar to age estimates obtained by other radiometric techniques, ranging between 160 and 600 Ma (Table 3). The main problem seems that a reliable ^{40}Ar-^{39}Ar age determination is precluded by the presence of Cl-derived ^{38}Ar. Indeed, we measured non-irradiated pyroxene and maskelynite separates that have significantly higher $^{36}Ar/^{38}Ar$ ratios in comparison with the irradiated samples. A higher Cl-derived ^{38}Ar component in the maskelynite separate could also explain the on average higher apparent ages in the age spectrum (Fig. 8) than for the whole rock sample, because this would lead to an underestimation of trapped ^{36}Ar. In this study, the apparent ages of Shergotty samples cluster around ~400 Ma. The age of the maskelynite separate of ~370 Ma is our lowest age for this sample, and our best upper age limit. However, it does not provide an upper age limit as stringent as the value given by Bogard et al. (1979) of 254 ± 10 Ma (Table 3).

Zagami

In the maskelynite separate, K-derived ^{39}Ar and Ca-derived ^{37}Ar are concordantly released over a broad temperature range (800–1700 °C). The degassing pattern is very similar to Shergotty with three recognizable peaks at 1000 °C, 1300 °C, and 1600 °C (Fig. 1), consistent with the maskelynite degassing pattern of experimentally shocked terrestrial gabbro (Trieloff 1993). Except for the 900–1020 °C extractions, the ^{40}Ar release pattern has a similar shape to ^{39}Ar and ^{37}Ar release patterns indicating that most of ^{40}Ar was produced by in situ decay of ^{40}K, or that excess argon is remarkably homogeneously distributed in the maskelynite. The $^{36}Ar/^{38}Ar$ ratios are lower than 0.7 for all temperature extractions due to Cl-induced ^{38}Ar, apart from the first one, which obviously contains a terrestrial atmospheric component. Apparent ages decrease with extraction temperature (Fig. 11a), similar to SaU 005 and Shergotty feldspar separates. The age spectrum has a minimum apparent age of 198 Ma that is slightly higher or similar to previously reported ages for Zagami samples (Table 3). One possibility is that excess ^{40}Ar trapped during formation causes this type of age spectrum, as recently suggested by Bogard and Park (2007b). Assuming a Zagami age of ~180 Ma, all temperature extractions contain a trapped component with $^{40}Ar/^{36}Ar$ ratios ~300–700.
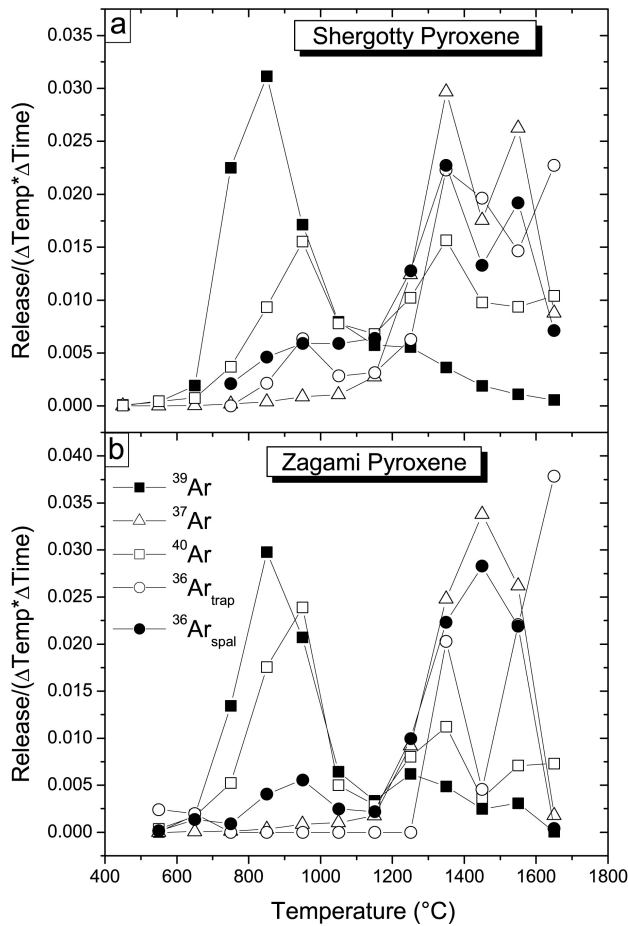
Fig. 9. Degassing patterns of argon isotopes of Shergotty (a) and Zagami (b) pyroxenes. While ^{37}Ar release at 1300–1500 °C is related to pyroxene degassing, the ^{39}Ar release peaks at 700–1000 °C are very probably related to minor K-bearing phases, e.g., magmatic melt inclusions within pyroxenes. In the pyroxene of Shergotty, this temperature range displays a release peak of trapped ^{36}Ar with high $^{40}Ar/(^{36}Ar)_{trapped}$ ratios.

The $^{36}Ar/^{38}Ar$ ratios of the pyroxene separate extractions are predominantly below the cosmogenic value, again indicating disturbance by Cl-produced ^{38}Ar. At 1200–1600 °C, Ca-derived ^{37}Ar is released from pyroxene (Fig. 9b). This is accompanied by concomitant release of a major portion of trapped ^{36}Ar. Most of ^{39}Ar and ^{40}Ar degas at 700–1100 °C, apparently from minor K-bearing phases, e.g., magmatic melt inclusions within pyroxene (Meyer 2007). The K/Ca spectrum (Fig. 11) confirms incongruent degassing of phases with considerably different K/Ca ratios. However, the ^{39}Ar release is not correlated exactly with the ^{40}Ar release between 700–1100 °C. These extractions have high $(^{40}Ar/^{36}Ar)_{total}$ ratios. For example, the 850 °C step shows $(^{40}Ar/^{36}Ar)_{total} = 1750 \pm 270$ and a high $^{36}Ar/^{37}Ar$ ratio of 0.017 indicating the presence of a significant trapped component. Contrary to the maskelynite separate, the age spectrum of this sample demonstrates stepwise increasing apparent ages (Fig. 11a). The lowest apparent age is ~290 Ma for the extraction 750 °C.
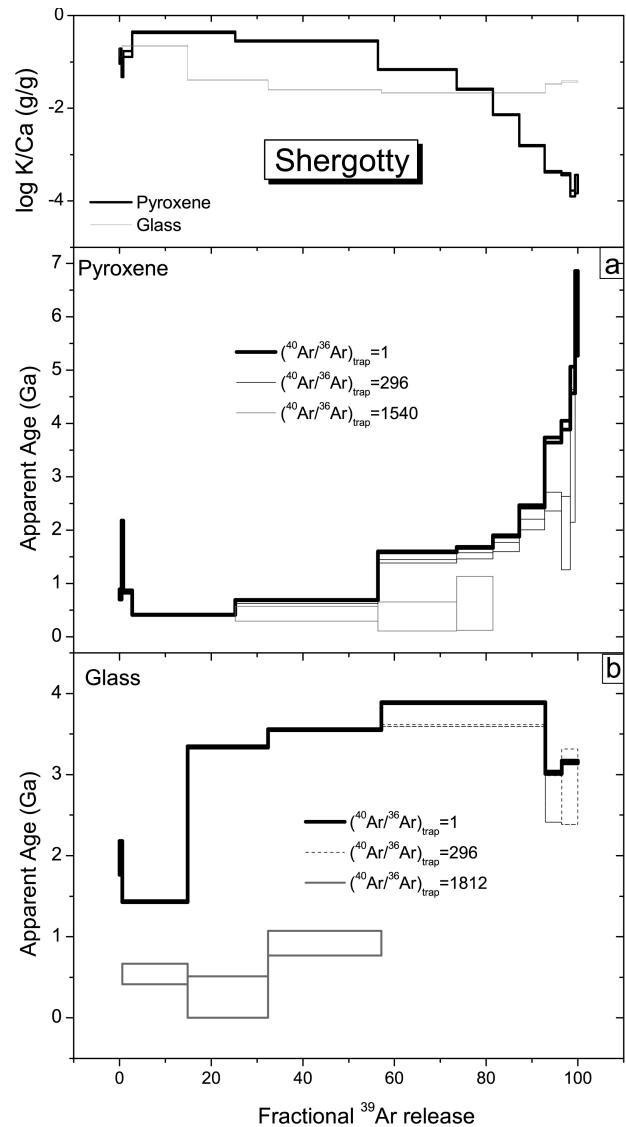
Fig. 10. K/Ca and age spectra of Shergotty pyroxene and glass. Correction for trapped components revealed by the three isotope plot significantly decreases excessively high apparent ages of the glass spectrum.

With a minimum $^{36}Ar/^{37}Ar$ ratio of 0.0011 for 1450 °C in order to decompose $^{36}Ar_{cosmogenic}$ and $^{36}Ar_{trapped}$ we obtain $^{40}Ar_{total}/^{36}Ar_{trapped}$ ratios ~1300–2000 for the 850–1250 °C temperature fractions and <750 for temperature extractions above 1300 °C. Apparent ages up to 1300 Ma in the age spectrum suggest that this sample contains possibly excess argon or inherited argon. The presence of trapped argon is supported by analyses of the non-irradiated pyroxene separate, for which the $^{36}Ar/^{38}Ar$ ratio of all temperature fractions are >0.65 and 2.1–3.5 for intermediate temperature extractions (850–1150 °C). This confirms that the irradiated pyroxene separate contains a significant amount of trapped argon, masked by Cl-produced ^{38}Ar.

Due to the low sample weight of the "opaque" separate (the exact identification is uncertain, but impact glass
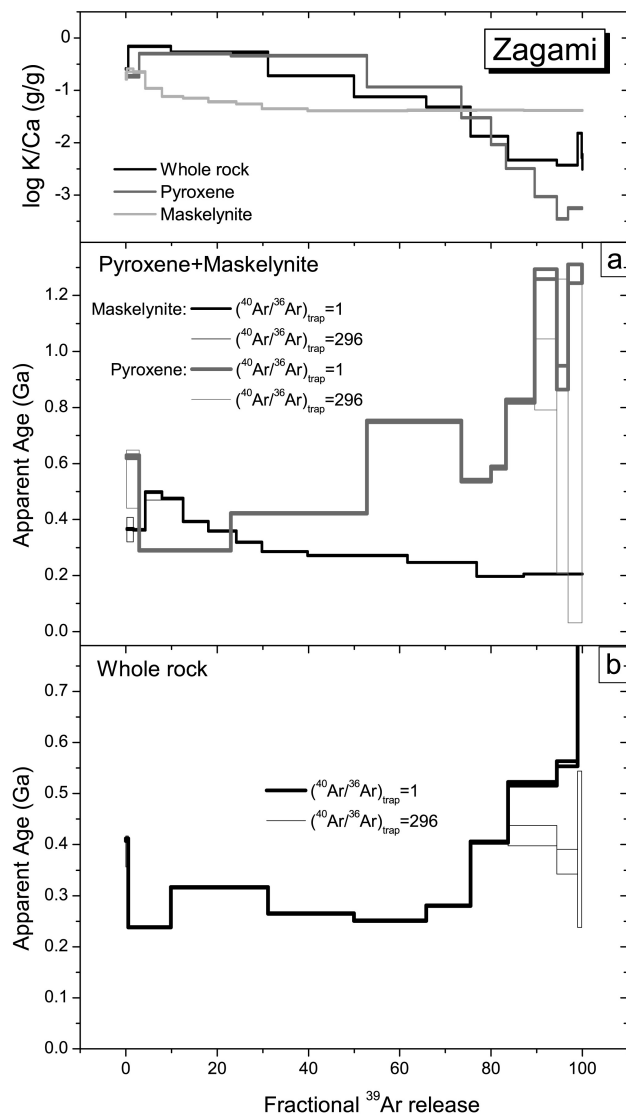
Fig. 11. K/Ca and age spectra of Zagami samples. The whole rock age spectrum can be explained by a superposition of maskelynite and pyroxene separate age spectra.

certainly contributed), only a limited number of temperature steps were performed. The ^{39}Ar and ^{37}Ar release patterns (Table A18) suggest the presence of different K- and Ca-bearing phases. The ^{40}Ar and $^{36}Ar_{trapped}$ release peaks coincide with the ^{37}Ar peak at ~1400 °C. The total concentration of 9.63 10^{-8} cm^3 STP/g ^{36}Ar is the highest value among the measured Zagami samples. The high $^{36}Ar/$ ^{38}Ar ratios (~2), $^{36}Ar/^{37}Ar$ ratios and apparent ages additionally demonstrate the presence of considerable amounts of trapped argon with high $^{40}Ar_{total}/^{36}Ar_{trapped}$ ratios close to ~1000, residing in a Ca-bearing retentive phase.

In the whole rock sample, the $^{36}Ar/^{38}Ar$ ratios within 750–1250 °C temperature interval are <0.65. A trapped component is definitely present in the high temperature fractions above 1250 °C, as judged by $^{36}Ar/^{38}Ar$ ratios from

0.8 to 4.3. The $^{36}Ar/^{37}Ar$ ratios vary considerably with maximum values for the 650–850 °C temperature extractions. As revealed by the three isotope correlation plot, extractions >1250 C° contain a trapped component with a terrestrial air-like $^{40}Ar/^{36}Ar$ ratio and a radiogenic component with an age of ~400 Ma. The whole rock age spectrum can be explained by a superposition of maskelynite and pyroxene separate age spectra (Fig. 11b). It has a minimum apparent age of ~240 Ma.

Zagami Summary

The lowest apparent Ar-Ar ages obtained in this study on Zagami mineral separates range from 200–250 Ma and are comparable with previously measured Ar-Ar ages of Zagami of 210–260 Ma (Table 3). A more detailed interpretation is obscured by complex age spectra due to the presence of excess argon, which can explain the variations of ^{40}Ar-^{39}Ar age spectra in different studies (e.g., Bogard and Park 2007b). Apparent ^{40}Ar-^{39}Ar ages of Zagami are generally lower than for Shergotty. As for the Shergotty samples, the release of Cl-produced ^{38}Ar seems to be an important obstacle in deconvolution of radiogenic from trapped argon. Age estimates of different chronological methods (Table 3) cover an age range between 170 and 230 Ma, except for the very high Pb-Pb age of 4 Ga reported by Bouvier et al. (2005).

Cosmic-Ray Exposure Ages

The cosmic-ray exposure (CRE) ages of shergottite samples were calculated from the concentration of cosmogenic ^{38}Ar. Total ^{38}Ar was corrected for a trapped component with both $(^{36}Ar/^{38}Ar)_{trapped}$ of 5.35 and 4.0. The calculated amounts of cosmogenic ^{38}Ar are an upper limit because of the possible presence of Cl-derived ^{38}Ar. We employed the production rate method for cosmogenic ^{38}Ar by Eugster and Michel (1995) using chemical compositions from previous studies (Stolper and McSween 1979; Stöffler et al. 1986; Lodders 1998; McSween and Treiman 1998; Dreibus et al. 2000; Gnos et al. 2002; Taylor et al. 2002). For SaU 005 production rate calculations, we applied chemical compositions of mineral phases of shergottite SaU 094, which is considered to be paired with SaU 005 (Gnos et al. 2002). No shielding correction was applied for the ^{38}Ar production rate, as it seems negligible for Martian meteorites (Eugster et al. 1997). The CRE ages of the most interesting samples are presented here as stepwise release age spectra (Figs. 12–14). The details of plotting CRE age spectra and the advantages of this kind of presentation are described in Korochantseva et al. (2005). Tables 1 and 3 summarize obtained CRE ages and applied production rates in this study and CRE ages from other studies.

CRE age spectra of Dhofar 019 pyroxene and maskelynite are highly concordant and flat over >70% of the ^{37}Ar release (Fig. 12), indicating no secondary diffusive losses of
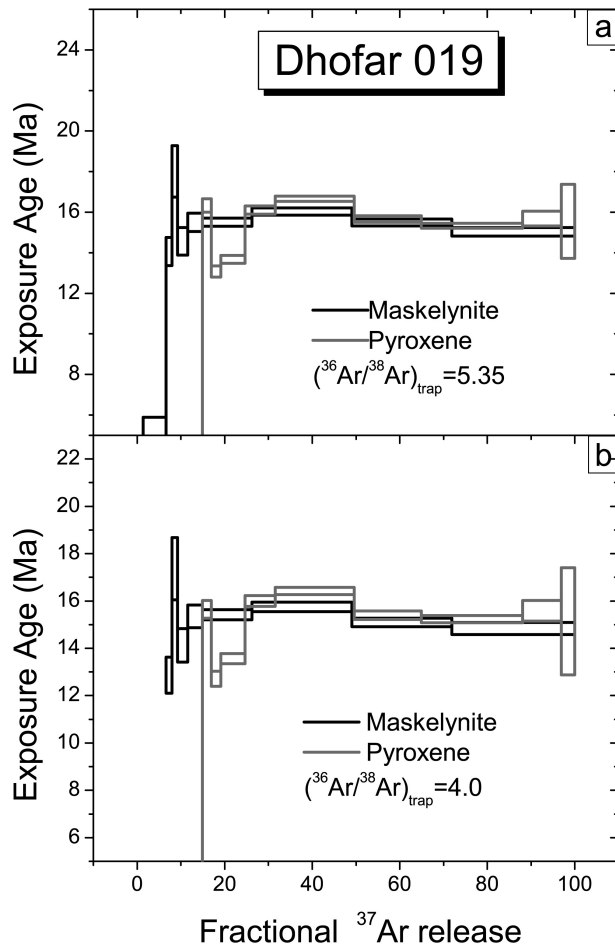
Fig. 12. CRE age spectra of pyroxene and maskelynite of Dhofar 019 calculated using $(^{36}Ar/^{38}Ar)_{trap}$ of 5.35 (a) and 4.0 (b). The CRE age spectra of these samples are highly concordant.

cosmogenic argon. Moreover, the agreement between the two mineral spectra supports the validity of the production rate calculations from the chemically different pyroxene and maskelynite, particularly considering their different concentration of the target elements Ca, Fe, K, etc., from which cosmogenic argon is produced. The average CRE ages of maskelynite and pyroxene are 15.8 ± 1.0 and 15.6 ± 1.0 Ma using $(^{36}Ar/^{38}Ar)_{trapped}$ = 5.35 and 4.0, respectively. The uncertainties of the CRE ages averaged from maskelynite and pyroxene include the variability of CRE ages from different mineral separates and, hence, include to a certain extent the individual production rate uncertainties adopted for maskelynite and pyroxene. However, systematic production rate uncertainties affecting production from different target elements in the same way cannot be included. Within these limitations we consider these values more accurate than previous CRE ages calculated from the total amount $^{38}Ar_{cos}$ of whole rock samples (Table 3). Then it is worth noting here that one of the SNC meteorites, ALH 84001, has also an old ejection age of 15.0 ± 0.8 Ma (Nyquist et al. 2001) which is
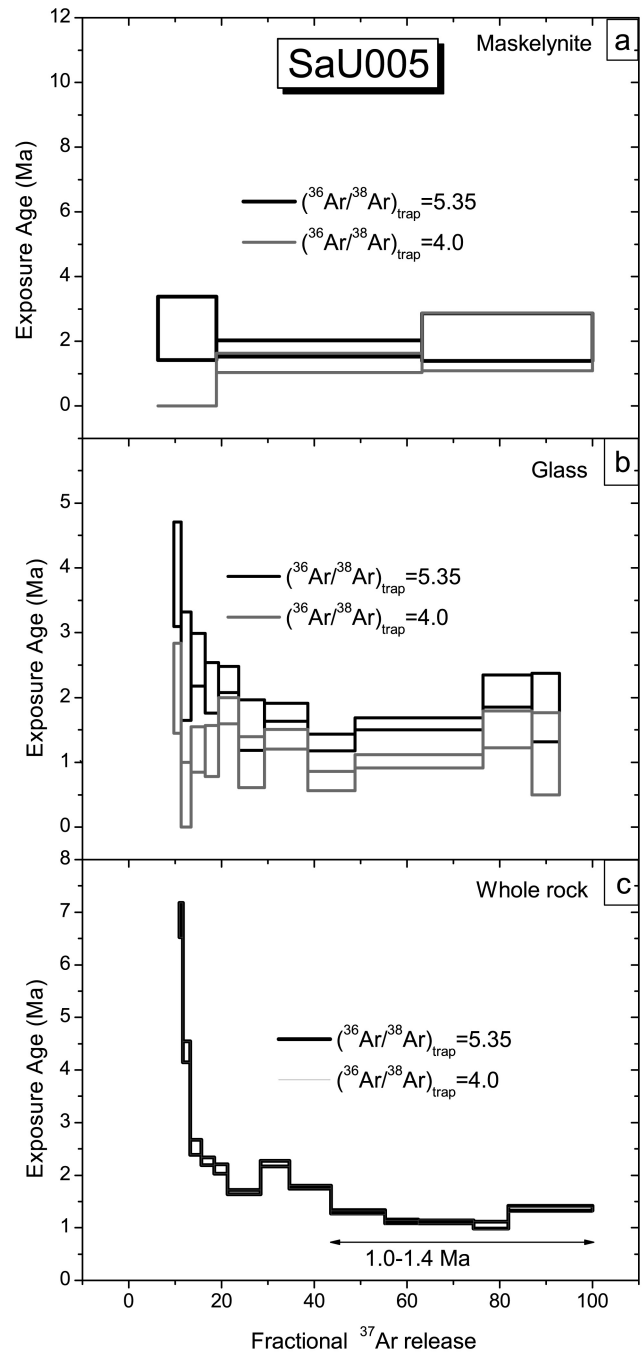
Fig. 13. CRE age spectra of SaU 005 maskelynite (a), glass (b) and whole rock (c). The CRE age of glass separate considerably depends on the trapped argon composition.

similar within uncertainty to the Dhofar 019 ejection age of 16.0 ± 0.7 Ma (the sum of our average cosmic ray exposure age of 15.7 ± 0.7 Ma and the terrestrial age of 0.34 ± 0.04 Ma).

The CRE age spectrum of SaU 005 maskelynite has high uncertainties. The individual extractions have CRE ages ≥1.4 Ma for $(^{36}Ar/^{38}Ar)_{trapped}$ = 5.35 and ≥1.0 Ma for $(^{36}Ar/^{38}Ar)_{trapped}$ = 4.0 (Fig. 13a). The CRE age calculation of

Fig. 14. CRE age spectra of Shergotty and Zagami samples. a) Age spectra which show CRE ages similar to previously published ages. b) The CRE age spectrum of Shergotty glass crucially depends on the $^{36}Ar/^{38}Ar$ ratio of the trapped argon component. c) Maskelynite age spectra display overestimated CREs due to significant contributions by Cl-derived ^{38}Ar.

SaU 005 glass requires knowledge of its chemical composition which is controlled by the local mineralogy. Only larger melt pockets can be expected to reach near bulk-rock composition (Gnos et al. 2002). The heterogeneous glass composition contributes additional uncertainty to the CRE age estimates.

Additional uncertainties are imposed from the choice of the isotopic composition of trapped argon: several extractions of the CRE age spectra corrected using different $(^{36}Ar/^{38}Ar)_{trapped}$ ratios of 5.35 and 4.0 are not consistent within uncertainties (Fig. 13b). We determine the glass CRE age to ~1.6 Ma for $(^{36}Ar/^{38}Ar)_{trapped} = 5.35$ and of ~1 Ma for $(^{36}Ar/^{38}Ar)_{trapped} = 4.0$. Release patterns of the whole rock sample show that the degassing of mineral phases mainly occurs at high temperatures. Hence, the CRE ages of 1.0–1.4 Ma of the extractions releasing 44–100% of the ^{37}Ar with $^{36}Ar/^{38}Ar$ >0.65 (Fig. 13c) can be considered as plausible, as all minerals with relevant target element concentrations contribute. The CRE ages of SaU 005 calculated from cosmogenic ^3He, ^{21}Ne and ^{38}Ar by Eugster et al. (2002) are 0.86 ± 0.13, 0.75 ± 0.12 and 1.06 ± 0.15 Ma, respectively (Table 3). Cosmic-ray exposure ages using cosmogenic ^3He, ^{21}Ne and ^{38}Ar published by Park et al. (2003) are 0.78–1.27 Ma (Table 3). They also estimated the ejection age from ^{81}Kr-^{83}Kr dating to 0.81 Ma. From own and literature data (Table 3) Eugster et al. (2002) give a preferred CRE age for SaU 005 to 1.2 ± 0.3 Ma.

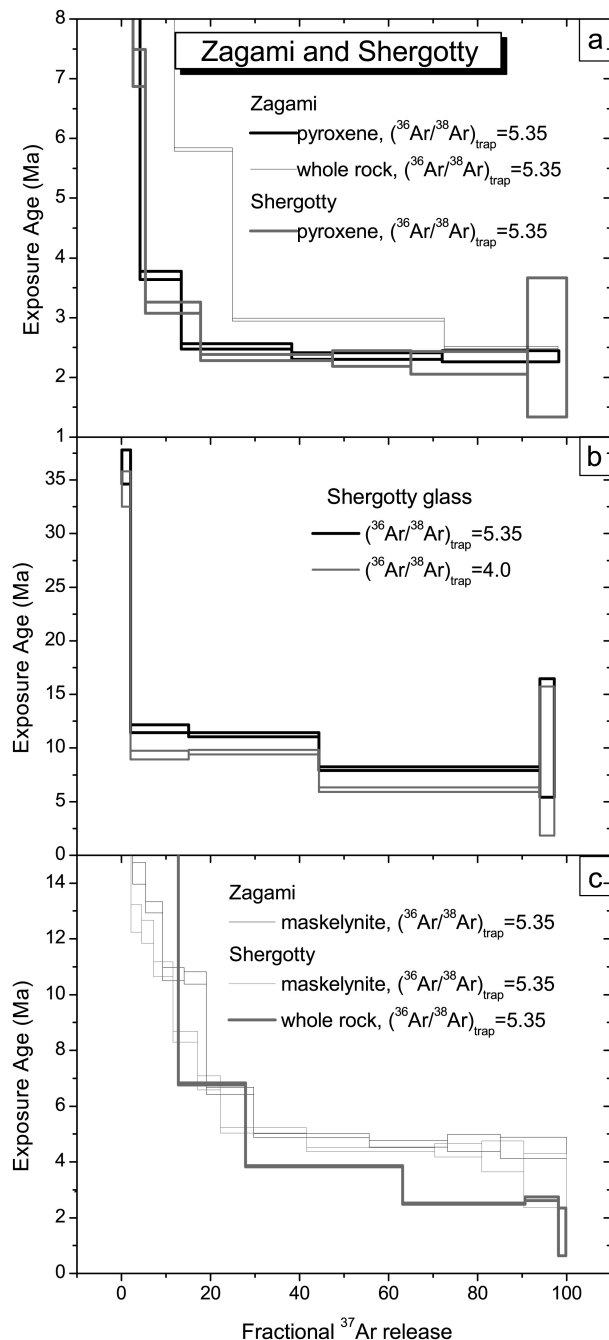The CRE age spectra of Shergotty pyroxene, Zagami pyroxene and Zagami whole rock (Fig.14a) yield ages of 2.1–2.5 Ma for 18–91% ^{37}Ar release, of 2.2–2.5 Ma for 13–98% ^{37}Ar release and of 2.4–3.0 Ma for 25–98% ^{37}Ar release, respectively. These ages agree with numerous results published previously (e.g., Eugster et al. 2002; Park et al. 2003; Schwenzer et al. 2007; Table 3). The heterogeneous composition of Shergotty glass precludes calculating a reliable CRE age. It should be noted that the CRE age calculation of this sample significantly depends on the trapped argon composition (Fig. 14b), as is the case for SaU 005 glass. Zagami maskelynite, Shergotty maskelynite, and Shergotty whole rock yield nominal CRE ages of up to 5 Ma at high extraction temperatures and are systematically overestimated due to significant contributions by Cl-derived ^{38}Ar (Fig. 14c).

^{39}Ar Release

All studied shergottites are severely shocked. In these meteorites plagioclase experienced intense structural changes during the shock event which resulted in formation of maskelynite. Previous data on ^{40}Ar-^{39}Ar dating of meteorites with high shock stages (Bogard et al. 1976; Bogard and Hirsch 1980; Kunz et al. 1995, 1997; Bogard and Garrison 1999; Korochantseva et al. 2007) and experimentally shocked plagioclase (Trieloff 1993, 1994b) suggests that a complex high temperature release pattern is a consequence of high-pressure transformation of plagioclase. Indeed, the release patterns of all Dhofar 019 and SaU 005 samples, Zagami and Shergotty maskelynites, and Shergotty glass separate show a high temperature, in most cases complex release of ^{39}Ar derived from K (Fig. 1). Another remarkable feature is elevated K/Ca ratios of Zagami and Shergotty maskelynite in

initial extractions, similar to experimentally shocked plagioclase (Trieloff 1993, 1994b), indicating some K redistribution process during the shock event.

Zagami and Shergotty pyroxene separates degas significant amounts of K-derived ^{39}Ar at 850 °C (Fig. 9). Such amounts of K cannot reside in the pyroxene mineral lattice. The most likely carrier phases are magmatic melt inclusions which are observed in Zagami and Shergotty pyroxenes (Meyer 2007), and were indeed found to be K-rich in the case of Shergotty (Nyquist et al. 1979a). By analogy, in Zagami pyroxene and whole rock, the main ^{39}Ar release peak is likely dominated by these inclusions.

The Ca and K concentrations of all whole rocks (Dhofar 019, SaU 005, Shergotty, and Zagami) inferred from K-derived ^{39}Ar and Ca-derived ^{37}Ar are in perfect agreement with other bulk analyses like X-ray fluorescence spectroscopy, atomic absorption, or instrumental neutron activation analysis (Table 2).

Trapped Argon in Shergottites

^{40}Ar/^{36}Ar Ratio of Trapped Argon from Martian Atmosphere and Interior

A ^{40}Ar/^{36}Ar ratio of 3000 ± 500 was determined by Viking for Martian atmospheric argon (Owen 1992) and hence the high ^{40}Ar/^{36}Ar ratios found in shergottites (Bogard and Johnson 1983) are usually interpreted as atmospheric argon trapped from the recent Martian atmosphere. With time, isotopic data on shergottites were gradually changing the scientific view about Martian atmospheric argon. For instance, Bogard and Garrison (1999) suggested that atmospheric argon has ^{40}Ar/^{36}Ar no greater than ~1900, substantially different from the Viking measurements. But there is no generally accepted certain value of the ^{40}Ar/^{36}Ar ratio for the Martian atmosphere so far.

High ^{40}Ar/^{36}Ar ratios of 1000–3000 were found for argon in Elephant Moraine (EET) A79001 (e.g., Bogard and Johnson 1983; Garrison and Bogard 1998), Zagami (Marti et al. 1995; Schwenzer et al. 2007), Shergotty (Bogard and Garrison 1999; Schwenzer et al. 2007; this study) and SaU 005 (Mohapatra and Ott 2000; this study). Many studies inferred the presence of atmospheric components from high ^{40}Ar$_{total}$/^{36}Ar$_{trapped}$ ratios only, i.e., not corrected for in situ radiogenic ^{40}Ar or inherited ^{40}Ar, or only with a rough correction for radiogenic argon based on K concentrations—which are variable. On the other hand, Ar-Ar isochron analysis appropriately corrected for cosmogenic and Cl-derived argon is a powerful tool to unequivocally identify a trapped high ^{40}Ar/^{36}Ar component (e.g., Bogard and Garrison 1999; this work). However, this correction is also not without drawbacks: For example, Bogard and Garrison (1999) used a method to resolve cosmogenic ^{36}Ar suggesting the application of the lowest ^{36}Ar/^{37}Ar ratio of the sample. This approach is restricted in a sense, that it can be used mainly for mineral separates from which cosmogenic isotopes—produced from different target elements (Ca, Fe, K)—are released congruently, thereby neglecting incongruently degassing impurities or inclusions. Moreover, the fraction with the minimum ^{36}Ar/^{37}Ar ratio may still contain trapped Ar. Resolving cosmogenic argon and trapped argon by using endmember compositions based on ^{36}Ar/^{38}Ar ratios (as mainly done in this study) is also not unproblematic due to the presence of Cl-derived argon in Ar-Ar dating. Principally, this could be quantified by simultaneous measurements of unirradiated samples. For example, the ^{36}Ar/^{38}Ar ratios of non-irradiated Shergotty pyroxene are significantly higher than those of the irradiated sample.

High (^{40}Ar/^{36}Ar)$_{trapped}$ ratios (Table 1) in our study were found for Shergotty pyroxene melt inclusions (~1500), however, these are likely overestimated due to Cl-induced ^{38}Ar. Similarly, (^{40}Ar/^{36}Ar)$_{trapped}$ ratios of 2000 for Shergotty pyroxene reported by Schwenzer et al. (2007) may be overestimated, as only the K content of pyroxene crystals was used to calculate in situ radiogenic argon, instead of the bulk K content of the separate, which is—as in our case—very likely dominated by K-rich melt inclusions in pyroxene and hence, may be significantly variable from sample to sample. While these considerations just advise to caution about uncertainties of (^{40}Ar/^{36}Ar)$_{trapped}$ values, it is ascertained that high (^{40}Ar/^{36}Ar)$_{trapped}$ ratios are reality. In this study, highest (^{40}Ar/^{36}Ar)$_{trapped}$ ratios (Table 1) were also found for Shergotty glass (~1800), maskelynite (~1200), and SaU 005 glass (~1200). Taken at face, these results are compatible with above mentioned studies, but our cautionary remarks above should be kept in mind.

Another important point is related to the identification of the high (^{40}Ar/^{36}Ar)$_{trapped}$ component as Martian atmospheric argon, which has become ambiguous: Schwenzer et al. (2007) found that only a very small proportion of the high (^{40}Ar/^{36}Ar)$_{trapped}$ argon is accompanied by Martian atmospheric xenon with high ^{129}Xe/^{132}Xe ratios. Indeed, most of the high (^{40}Ar/^{36}Ar)$_{trapped}$ argon component must be ascribed to the Martian interior. Similarly, Bogard and Park (2007b) assigned the high ^{40}Ar/^{36}Ar excess argon found in Zagami maskelynite to a magmatic component inherited from the Martian interior, and our results are as well consistent with these conclusions. Until recently, Martian mantle argon was considered to have low ^{40}Ar/^{36}Ar ratios: For instance, Wiens (1988) estimated the ^{40}Ar/^{36}Ar ratio of the mantle component present in EETA79001 to be between 430 and 680, Swindle et al. (1986) suggested a component in the same meteorite with ^{40}Ar/^{36}Ar <300, Bogard and Garrison (1999) concluded a ^{40}Ar/^{36}Ar ratio of <500 for the Martian mantle. Taking all results into account, Martian interior (or mantle) argon may be characterised by very distinct heterogeneous compositions. Incidentally, this was also recently inferred for the terrestrial lithospheric mantle, where mantle argon (evaluated by

correlations with solar type neon) in different lithospheric samples was found to have highly variable $^{40}Ar/^{36}Ar$ ratios (Hopp et al. 2007).

Incorporation of Trapped Argon

Atmospheric noble gases are ubiquitous on Earth and noble gas geochemists perform huge efforts to search rocks not contaminated by atmospheric gases with pristine mantle noble gases. Contrary, Martian atmospheric gases are rarely found in SNC meteorites and—in shergottites—generally attributed to shocked phases, incorporated somehow by the shock process (Bogard and Johnson 1983; Terribilini et al. 1998). It was suggested that the scatter in "Martian atmospheric" $^{40}Ar/^{36}Ar$ ratios determined in different shergottites is related to the shock pressure of shergottites and could be due to the mixture of different components (e.g., Martian atmosphere and mantle) and their inhomogeneous distribution (Bogard and Garrison 1998; Terribilini et al. 1998). However, there is no definite correlation between shock pressures and the $^{40}Ar/^{36}Ar$ ratios of trapped argon: For example, the glass sample from SaU 005, a heavily shocked shergottite (40–45 GPa; Fritz et al. 2005), contains a trapped component with $^{40}Ar/^{36}Ar$ of ~1200, while Shergotty experienced a lower shock pressure (30.5 ± 2.5 GPa; Fritz et al. 2005) and shows $(^{40}Ar/^{36}Ar)_{trapped}$ ratios up to 1800 (Bogard and Garrison 1999; this study). Moreover, analyses of the same EET79001,27 inclusion conducted by different laboratories demonstrate a wide range of $(^{40}Ar/^{36}Ar)_{trapped}$ ratios (Bogard and Garrison 1998). In particular for Shergotty, our own data and those by Bogard and Garrison (1999) display data almost linearly aligned in a three isotope plot (Fig. 7). If the trapped component with $^{40}Ar/^{36}Ar$ of ~1200 is a mixture of Martian atmosphere and mantle, and the result of shock implantation, this would require equilibration of atmospheric and mantle argon mobilized during the impact. If mantle argon was not mobilized during the impact and equilibrated with Martian atmospheric argon, we would expect different phases hosting the two trapped components with likely different degassing behavior. This would result in a scatter of data plotting in a triangle between one radiogenic and two trapped compositions in a plot of $^{36}Ar_{trapped}/^{40}Ar_{total}$ versus $^{39}Ar/^{40}Ar_{total}$, as is indeed observed for many shergottite samples (Bogard and Garrison 1999; this study). To explain the linear Shergotty data, we suggest to consider a different possibility, that the high $(^{40}Ar/^{36}Ar)_{trapped}$ ratios found are not from "true" Martian atmosphere but could be implanted from an "impact-generated" transient atmosphere. A recent study on L chondrites (Korochantseva et al. 2007) demonstrated that capture of gases from a temporal atmosphere is possible. Any addition of mobilized gases from crustal or mantle rocks during impact could significantly increase the $^{40}Ar/^{36}Ar$ ratio of trapped argon.

The mineral separates of olivine-phyric shergottites Dhofar 019 and SaU 005 (except for the SaU 005 glass)

display low $^{40}Ar/^{36}Ar_{trapped}$ ratios of 300–400. Such an ubiquitous occurrence of trapped argon with low $^{40}Ar/^{36}Ar_{trapped}$ ratios can be interpreted as Martian mantle component (Wiens 1988; Swindle et al. 1986; Bogard and Garrison 1999) or explained by a possible terrestrial contamination (cf. Marty et al. 2006). Cleaning and grinding related to sample preparation can incorporate terrestrial Ar into already contaminated desert meteorites, however, atmospheric Ar is commonly released at low temperatures below 750 °C (Korochantseva et al. 2005). These extractions were omitted for the evaluation of the isotopic composition of trapped argon in this study. Nevertheless, the observation that the uncorrected age spectra of mineral separates of SaU 005 show higher ages than the whole rock spectrum at intermediate to high temperatures is confusing and could hint at very retentively bound trapped argon of terrestrial origin introduced by mineral separation procedures. For maskelynite and pyroxene of Dhofar 019, uncorrected ages are only marginally higher than for the whole rock sample, while the uncorrected ages of Shergotty and Zagami maskelynite are higher in extractions up to 1250 °C and 1100 °C, respectively. This is again a possible indication for contamination by terrestrial atmospheric argon, or alternatively, an insufficient correction for trapped ^{40}Ar, due to underestimation of trapped ^{36}Ar by a Cl-derived ^{38}Ar component (see above). However, the seven Shergotty maskelynite extractions between 850 °C and 1250 °C belong to the linear array in Fig. 7 that points to argon with a high $(^{40}Ar/^{36}Ar)_{trapped}$ ratio of 1200. Hence, this excess argon cannot be of terrestrial atmospheric origin. Similarly, $(^{40}Ar/^{36}Ar)_{trapped}$ ratios identified for Dhofar 019 samples are distinctly higher than the terrestrial atmospheric ratio. Garrison and Bogard (2001) also found low $(^{40}Ar/^{36}Ar)_{trapped}$ ratios for Dhofar 019 samples, and presumed that it is a trapped Martian interior argon. The trapped xenon of Dhofar 019 indicates both Martian atmosphere and mantle components (Shukolyukov et al. 2002). Thus, we conclude that the low $(^{40}Ar/^{36}Ar)_{trapped}$ ratios of 300–400 for Dhofar 019 and SaU 005 can be ascribed to indigeneous Martian component(s) rather than terrestrial contamination although we cannot completely exclude the latter, in particular for SaU 005.

$^{36}Ar/^{38}Ar$ Ratio of Trapped Argon

The trapped Martian component characterized by a high $^{40}Ar/^{36}Ar$ ratio was inferred to have a low $^{36}Ar/^{38}Ar$ ratio of ≤4.0 (e.g., Bogard 1997; Garrison and Bogard 1998) or 4.1 ± 0.2 (Wiens et al. 1986). Precise determination of the isotopic compositions of trapped argon components in Martian meteorites is very important to test the genetic relationship between Martian mantle and atmosphere and to constrain the atmospheric evolution. A compellingly low $^{36}Ar/^{38}Ar$ component remains to be verified in other shergottites than EETA79001. Two circumstances would favor the

determination of an accurate $(^{36}Ar/^{38}Ar)_{trapped}$ ratio in SNCs: the low CRE age of a specific meteorite (minimizing cosmogenic ^{38}Ar) and a high concentration of trapped argon which is preferentially found in shock phases. Our results demonstrate (e.g., Figs. 13b and 14b) that calculated CRE ages of shock phases (SaU 005 and Shergotty glasses) seriously depend on the $^{36}Ar/^{38}Ar$ ratio of trapped argon, in contrast to other samples for which the exact choice of the $(^{36}Ar/^{38}Ar)_{trapped}$ ratio is not crucial. However, the heterogeneous chemical composition of shock phases unfortunately contributes a high uncertainty to the CRE age calculation that prevents the accurate identification of the $(^{36}Ar/^{38}Ar)_{trapped}$ ratio. Moreover, if argon with high $^{40}Ar/^{36}Ar$ ratios was implanted into shocked phases from a local impact induced "transient atmosphere," it would be very difficult to properly constrain the $^{36}Ar/^{38}Ar$ ratio of the Martian atmosphere based on the argon composition from such impact glasses.

Young or Old Shergottites?

The young Rb-Sr, Sm-Nd and ^{40}Ar-^{39}Ar ages of shergottites are usually regarded as crystallization ages (Nyquist et al. 2001). Indeed, this was and is one of the strongest arguments for the origin of SNC meteorites from Mars. Currently, there are strong debates about the interpretation of young Rb-Sr, Sm-Nd and ^{40}Ar-^{39}Ar ages of shergottites, envisaging much older crystallization ages: Bouvier et al. (2005) suggested the young radiometric ages (U-Pb, Rb-Sr, Sm-Nd, and Lu-Hf) of basaltic shergottites could be related to the activity of acidic aqueous solutions on the Martian surface, while their reported ancient Pb-Pb age of ~4 Ga would correspond to the magmatic emplacement of these rocks. Such ancient crystallisation ages could potentially remove the discrepancy between predominantly young radiometric ages of Martian meteorites and much older ages of the Martian surface derived from impact crater counting statistics (Nyquist 2006), and also explain the existence of variable extinct radioactive nuclide anomalies (Foley et al. 2005).

For Ar-Ar chronology, this scenario would have important consequences, as part of the excess ^{40}Ar ascribed to incorporation from external sources could principally be mere inherited ^{40}Ar, i.e., radiogenic argon incompletely degassed during secondary events. Although the Ar-Ar system may have hardly been reset by percolating fluids, it could suffer from impact metamorphism. On the other hand, at least some shergottites show remarkably similar Rb-Sr, Sm-Nd and ^{40}Ar-^{39}Ar ages, for example, Dhofar 019 or NWA 1460 (Bogard and Park 2007a). This favors the young igneous formation scenario, as Rb-Sr, Sm-Nd and ^{40}Ar-^{39}Ar chronometers should experience different degrees of isotopic resetting during secondary events which would result in different, not similar ages. Nevertheless, there remains the principal possibility that Rb-Sr and Sm-Nd chronometers can be reset to the same degree as the ^{40}Ar-^{39}Ar system in the case of

powerful impact events and massive heating events as, e.g., observed in L chondrites (e.g., Chico, Point of Rocks; Nakamura et al. 1990; Bogard et al. 1995; Korochantseva et al. 2007). At the dawn of Martian meteorite investigations, young radiometric ages were just regarded in the context of impact resetting (Nyquist et al. 1979b). Although shergottites are severely shocked rocks, Rb-Sr, Sm-Nd, and ^{40}Ar-^{39}Ar chronometers cannot suffer a major reset by shock effects unless intense post shock heating or melting is achieved. For example, conversion of feldspar to maskelynite causes only minor ^{40}Ar loss (Trieloff et al. 1994b). A complete reset by ^{40}Ar loss would require much stronger local shock wave effects (e.g., melt formation as observed for L chondrites; Bogard et al. 1995; Korochantseva et al. 2007) or substantial accompanying heating effects. Shergottites certainly experienced secondary heating in their histories, but was it sufficiently strong to modify isotopic characteristics of rocks? Mineralogical and petrological studies of shergottites usually demonstrate that these rocks were not exposed to any significant thermal events (changing rock textures and mineral compositions, causing formation of new minerals) and experienced only localized melting during or after the impact events ejecting them from Mars (Nyquist et al. 2001). In particular, Dhofar 019 has a basaltic texture and displays large compositional ranges of the minerals indicating relatively rapid cooling. As shock effects of individual SNC-meteorites are attributed to a single shock event (with the exception of ALH 84001), most likely the specific meteorite's ejection from Mars (Nyquist et al. 2001), this would mean that the ^{40}Ar-^{39}Ar age is not reset by the meteorite's ejection. The lack of indications of secondary impact reheating in many cases rather suggests the young ages to be primary formation ages, not due to a strong and powerful secondary reset.

In this context, it is worth to note that ^{40}Ar-^{39}Ar data of some shergottite samples linearly correlate in an isochron plot (Bogard and Garrison 1999; this study) revealing the composition of trapped argon and the radiogenic component. If trapped argon was incorporated during the last impact event, generally assumed to be the meteorite's ejection from Mars, and if the radiogenic component dates the crystallisation event, such a linear array would be a mixing-line and not an isochron sensu stricto. In the case of such low energetic secondary events, the agreement of the ^{40}Ar-^{39}Ar age with the Rb-Sr and Sm-Nd data would be the perfect argument that the ^{40}Ar-^{39}Ar age was not changed by the last impact event and is chronologically meaningful.

Meanwhile, the existing variations in radiometric ages—frequently discordant for individual SNC meteorites—do not allow to generally derive a simple one stage history of shergottites. For example, it appears that SaU 005 underwent at least two secondary events causing formation of glass and its recrystallization (see Schwenzer et al. 2002). Besides that, the minerals and glasses in SaU 094 (paired with SaU 005)

show little zonation implying that the minerals had enough time to chemically reequilibrate and the grain size of the groundmass is larger than in typical terrestrial volcanic flows (Gnos et al. 2002). Further concerted efforts are certainly required to unambiguously elucidate earlier primary and secondary events.

SUMMARY AND CONCLUSIONS

We analyzed whole rocks and mineral separates of Martian shergottites Dho 019, SaU 005, Shergotty, and Zagami using the ^{40}Ar-^{39}Ar technique. Isotope data were obtained by detailed stepwise degassing procedures on mineral separates, which enabled us to identify major and minor phases as carrier phases of trapped argon, e.g., high $(^{40}Ar/^{36}Ar)_{trapped}$ ratios (~1000–2000) were found in a variety of phases. We obtained the first Ar-Ar dating results for SaU 005, and complementary data for Dho 019, Shergotty, and Zagami. Although the multiplicity of argon components (trapped Martian atmosphere, Martian mantle, cosmogenic, terrestrial atmosphere, in situ radiogenic ^{40}Ar) make shergottite dating one of the most challenging tasks for ^{40}Ar-^{39}Ar chronologists and induce considerable uncertainties, it is, e.g., clear that SaU 005 and Dhofar 019 are quite similar to other shergottites in displaying relatively young ^{40}Ar-^{39}Ar ages, certainly <1 Ga old.

Shergottite samples containing maskelynite or shock-glass display complex argon release patterns typical of high-pressure phases. On the other hand, pyroxene separates from Shergotty and Zagami have a low-temperature release of ^{39}Ar dominated by K-rich magmatic melt inclusions, which also affect the release patterns of Shergotty and Zagami whole rock samples. We detected argon of unequivocal nonradiogenic, trapped origin with high $^{40}Ar/^{36}Ar$ ratios for Shergotty pyroxene of 1500, which could be ascribed to melt inclusions. Recently Schwenzer et al. (2007) have also found mantle argon with high $(^{40}Ar/^{36}Ar)_{trapped}$ ratios for Shergotty and Zagami pyroxenes. It follows that a high $(^{40}Ar/^{36}Ar)_{trapped}$ component usually ascribed uniquely to the Martian atmosphere can as well originate from the Martian interior (Bogard and Park 2007b; Schwenzer et al. 2007; this study). This provides new insight into the argon isotopic composition of the Martian mantle that may be more heterogeneously than previously thought (e.g., Swindle et al. 1986; Bogard and Garrison 1999).

High $(^{40}Ar/^{36}Ar)_{trapped}$ ratios were also found for Shergotty maskelynite (~1200) and for impact glasses from basaltic shergottite Shergotty (~1800) and the olivine-phyric shergottite SaU 005 (~1200). Argon with high $(^{40}Ar/^{36}Ar)_{trapped}$ ratios found in shock transformed phases of shergottites is commonly interpreted to be implanted from the Martian atmosphere, with possible minor contributions from Martian mantle. We suggest an additional explanation that the high $(^{40}Ar/^{36}Ar)_{trapped}$ ratios could be implanted into shergottite impact glasses from a temporary atmosphere

following the impact as recently demonstrated for L chondrites (Korochantseva et al. 2007). Such a temporary atmosphere could contain both degassed or remobilized radiogenic ^{40}Ar and ^{36}Ar (of primordial and possibly trapped solar origin).

All studied samples of Dhofar 019 and mineral separates of SaU 005 apart from glass (i.e., from olivine-phyric shergottites) display low $(^{40}Ar/^{36}Ar)_{trapped}$ ratios of 300–400 resembling a Martian mantle component usually considered to have low $^{40}Ar/^{36}Ar$ ratios (Swindle et al. 1986; Wiens 1988; Bogard and Garrison 1999).

The $^{36}Ar/^{38}Ar$ ratio of the Martian atmosphere—which is important for constraining atmospheric evolution—can be potentially determined from shock-induced phases enriched by trapped Ar of meteorites having low cosmic ray exposure ages. Studied SaU 005 and Shergotty glasses satisfy these requirements, however, the heterogeneous chemical composition of shock phases prevented the accurate identification of the $(^{36}Ar/^{38}Ar)_{trapped}$ ratio.

The variations in radiometric ages obtained by different methods for individual meteorites can principally reflect both internal methodological problems and the influence of real secondary geological processes acting on old crystallised rocks. The interpretation of chronological results strongly depends on mineralogical-petrological observations. The most vital question is if there had been more energetic (thermal and/or impact) events preceding the late excavation of shergottites from Mars. In view of existing mineralogical-petrological data the young Ar-Ar, Sm-Nd, Rb-Sr ages of most shergottites probably date the primary events. However, SaU 005 is likely to have experienced a secondary event induced by strong shock as well as thermal effects (see Schwenzer et al. 2002; Gnos et al. 2002) that must have affected isotopic systems. Indeed, high-temperature SaU 005 glass displays diffusional loss of argon.

We regard the Dhofar 019 maskelynite ^{40}Ar-^{39}Ar age of 642 ± 72 Ma as compatible with Sm-Nd and Rb-Sr ages (Borg et al. 2001) and as probable crystallization age. The ^{40}Ar-^{39}Ar age of melt inclusions within Dhofar 019 olivine megacrysts $(1086 \pm 252$ Ma) may represent the time of the entrapment of a magmatic liquid during crystallization. The ^{40}Ar-^{39}Ar age of SaU 005 olivine of 885 ± 66 Ma dominated by primary melt inclusions could be the crystallization age in the case if glass inclusions within the highly retentive olivine crystals were not influenced by secondary event(s) observed for this meteorite. However, ages of Dhofar 019 and SaU 005 olivines may be also meaningless if the high ages of glass inclusions simply reflect the presence of magmatic argon with a highly radiogenic signature. The age spectra of Shergotty and Zagami are influenced by excess argon: the presence of Cl-derived ^{38}Ar precludes proper quantification of trapped ^{36}Ar and, hence, obscures the chronological information. The lowest ^{40}Ar-^{39}Ar age of Shergotty was obtained for maskelynite and is ~370 Ma, higher than the apparent age of Zagami.

Both Shergotty and Zagami (and also olivine phyric shergottites) contain excess ^{40}Ar. This can be explained in terms of incorporated extraneous argon with high ^{40}Ar/^{36}Ar ratios (Martian or impact-induced atmosphere, Martian interior). We consider the alternative explanation—taking into account the recent suggestion by Bouvier et al. (2005) of extremely old shergottite crystallization ages—that ^{40}Ar is an inherited component accumulated previously and only incompletely lost during secondary event(s) as unlikely, because 1) excess ^{40}Ar can be identified via isochron plots and is usually supported by trapped ^{36}Ar, i.e., characterized by a certain ^{40}Ar /^{36}Ar ratio. Inherited ^{40}Ar would not be supported by (because not equilibrated with) trapped ^{36}Ar; 2) many individual temperature extractions provide ages >4.6, i.e., older than the solar system, which would not be the case if ^{40}Ar was inherited from in situ K-decay.

There remains the possibility that shergottites may represent a very unusual case in which many chronometers have been reset, and that only some very weak hints at an old crystallization history survived. To evaluate this possible—though perhaps unlikely—scenario, the present data base seems not to be sufficiently conclusive.

Cosmic-ray exposure ages determined from the concentration of cosmogenic ^{38}Ar are: 15.7 ± 0.7 Ma (Dhofar 019), ~1.0–1.6 Ma (SaU 005), 2.1–2.5 Ma (Shergotty), and 2.2–3.0 Ma (Zagami).

Editorial Handling—Dr. Timothy Swindle

REFERENCES

Badjukov D. D., Nazarov M. A., and Taylor L. A. 2001. Shock metamorphism in the shergottite meteorite Dhofar 019 (abstract #2195). 32nd Lunar and Planetary Science Conference. CD-ROM.

Becker R. H. and Pepin R. O. 1984. The case for a Martian origin of the shergottites: Nitrogen and noble gases in EETA79001. *Earth and Planetary Science Letters* 69:225–242.

Bogard D. D. 1997. A reappraisal of the Martian ^{36}Ar/^{38}Ar ratio. *Journal of Geophysical Research* 102:1653–1661.

Bogard D. D. and Hirsch W. C. 1980. ^{40}Ar/^{39}Ar dating, Ar diffusion properties, and cooling rate determinations of severely shocked chondrites. *Geochimica et Cosmochimica Acta* 44:1667–1682.

Bogard D. D. and Johnson P. H. 1983. Martian gases in an Antarctic meteorite? *Science* 221:651–654.

Bogard D. D. and Garrison D. H. 1998. Composition of Martian noble gases trapped in Martian meteorite impact glasses (abstract #1076). 29nd Lunar and Planetary Science Conference. CD-ROM.

Bogard D. D. and Garrison D. H. 1999. Argon-39-argon-40 "ages" and trapped argon in Martian shergottites, Chassigny, and Allan Hills 84001. *Meteoritics & Planetary Science* 34:451–473.

Bogard D. D. and Park J. 2007a. Ar-Ar age of NWA-1460 and evidence for young formation ages of the shergottites (abstract #1096). 38th Lunar and Planetary Science Conference. CD-ROM.

Bogard D. D. and Park J. 2007b. Excess ^{40}Ar in the Zagami shergottite: Does it reveal crystallization history? *Meteoritics & Planetary Science* 42:A21.

Bogard D. D., Garrison D. H., Norman M., Scott E. R. D., and Keil K. 1995. ^{39}Ar-^{40}Ar age and petrology of Chico: Large-scale impact melting on the L chondrite parent body *Geochimica et Cosmochimica Acta* 59:1383–1399.

Bogard D. D., Husain L., and Nyquist L. E. 1979. ^{40}Ar-^{39}Ar age of the Shergotty achondrite and implications for its post-shock thermal history. *Geochimica et Cosmochimica Acta* 43:1047–1055.

Bogard D. D., Husain L., and Wright R. J. 1976. ^{40}Ar-^{39}Ar dating of collisional events in chondrite parent bodies. *Journal of Geophysical Research* 32:5664–5678.

Borg L. E., Asmerom Y., and Edmunson J. E. 2003. Uranium-lead isotopic systematics of the Martian meteorite Zagami (abstract #1107). 34th Lunar and Planetary Science Conference. CD-ROM.

Borg L. E., Nyquist L. E., Reese Y., Wiesmann H., Shih C.-Y., Ivanova M., Nazarov M. A., and Taylor L. A. 2001. The age of Dhofar 019 and its relationship to the other Martian meteorites (abstract #1144). 32nd Lunar and Planetary Science Conference. CD-ROM.

Bouvier A., Blichert-Toft J., Vervoort J., and Albarede F. 2005. The age of SNC meteorites and the antiquity of the Martian surface. *Earth and Planetary Science Letters* 240:221–233.

Brereton N. R. 1970. Corrections for interfering isotopes in the ^{40}Ar/^{39}Ar dating method. *Earth and Planetary Science Letters* 8:427–433.

Chen J. H. and Wasserburg G. J. 1986. Formation ages and evolution of Shergotty and its parent planet from U-Th-Pb systematics. *Geochimica et Cosmochimica Acta* 50:955–968.

Chen M. and El Goresy A. 2000. The nature of maskelynite in shocked meteorites: Not diaplectic glass but a glass quenched from shock-induced dense melt at high pressures. *Earth and Planetary Science Letters* 179:489–502.

Dreibus G., Spettel B., Haubold R., Jochum K. P., Palme H., Wolf D., and Zipfel J. 2000. Chemistry of a new shergottite: Sayh al Uhaymir 005 (abstract). *Meteoritics & Planetary Science* 35:A49.

El Goresy A., Dubrovinsky L., Sharp T. G., Saxena S. K., and Chen M. 2000. A monoclinic post-stishovite polymorph of silica in the Shergotty meteorite. *Science* 288:1632–1634.

El Goresy A., Graup G., and Chen M. 2003. The assemblage maskelynite–post-stishovite silica polymorphs in the Shergotty meteorite: New stringent constraints to peak-shock pressures (abstract). *Meteoritics & Planetary Science* 38:A50.

Eugster O. and Michel Th. 1995. Common asteroid breakup events of eucrites, diogenites, and howardites and cosmic-ray production rates for noble gases in achondrites. *Geochimica et Cosmochimica Acta* 59:177–199.

Eugster O., Busemann H., Lorenzetti S., and Terribilini D. 2002. Ejection ages from krypton-81-krypton-83 dating and preatmospheric sizes of Martian meteorites. *Meteoritics & Planetary Science* 37:1345–1360.

Eugster O., Weigel A., and Polnau E. 1997. Ejection times of Martian meteorites. *Geochimica et Cosmochimica Acta* 61:2749–2757.

Foley C. N., Wadhwa M., Borg L. E., Janney P. E., Hines R., and

Grove T. L. 2005. The early differentiation history of Mars from ^{182}W-^{142}Nd isotope systematics in the SNC meteorites. *Geochimica et Cosmochimica Acta* 69:4557–4571.

Fritz J., Artemieva N., and Greshake A. 2005. Ejection of Martian meteorites. *Meteoritics & Planetary Science* 40:1393–1411.

Garrison D. H. and Bogard D. D. 2001. Argon-39-Argon-40 "ages" and trapped argon for three Martian shergottites (abstract). *Meteoritics & Planetary Science* 36:A62–63.

Garrison D. H. and Bogard D. D. 1998. Isotopic composition of trapped and cosmogenic noble gases in several Martian meteorites. *Meteoritics & Planetary Science* 33:721–736.

Geiss J. and Hess D. C. 1958. Argon-potassium ages and the isotopic composition of argon from meteorites. *The Astrophysical Journal* 127:224–236.

Gnos E., Hofmann B., Franchi I. A., Al-Kathiri A., Hauser M., and Moser L. 2002. Sayh al Uhaymir 094: A new Martian meteorite from the Oman desert. *Meteoritics & Planetary Science* 37: 835–854.

Hopp J. and Trieloff M. 2005. Refining the noble gas record of the Réunion mantle plume source: Implications on mantle geochemistry. *Earth and Planetary Science Letters* 240:573–588.

Hopp J., Trieloff M., Buikin A. I., Korochantseva E. V., Schwarz W. H., Althaus T., and Altherr R. 2007. Heterogeneous mantle argon isotope composition in the subcontinental lithospheric mantle of the Red Sea. *Chemical Geology* 240:36–53.

Huneke J. C. and Smith S. P. 1976. The realities of recoil: ^{39}Ar recoil out of small grains and anomalous patterns in ^{39}Ar-^{40}Ar dating. Proceedings, 7th Lunar Science Conference. pp. 1987–2008.

Jagoutz E. and Wänke H. 1986. Sr and Nd isotopic systematics of Shergotty meteorite. *Geochimica et Cosmochimica Acta* 50:939–953.

Jagoutz E., Dreibus G., Jotter R., Kubny A., and Zartman R. 2006. U-Pb data on clean minerals from nakhlites (abstract). *Meteoritics & Planetary Science* 41:A87.

Jessberger E. K., Dominik B., Staudacher Th., and Herzog G. F. 1980. ^{40}Ar-^{39}Ar ages of Allende. *Icarus* 42:380–405.

Korochantseva E. V., Trieloff M., Buikin A. I., Hopp J., and Meyer H.-P. 2005. $^{40}Ar/^{39}Ar$ dating and cosmic-ray exposure time of desert meteorites: Dhofar 300 and Dhofar 007 eucrites and anomalous achondrite NWA 011. *Meteoritics & Planetary Science* 40:1433–1454.

Korochantseva E. V., Trieloff M., Lorenz C. A., Buikin A. I., Ivanova M., Schwarz W. H., Hopp J., and Jessberger E. K. 2007. L-chondrite asteroid breakup tied to Ordovician meteorite shower by multiple isochron ^{40}Ar-^{39}Ar- dating. *Meteoritics & Planetary Science* 42:113–130.

Kunz J., Falter M., and Jessberger E. 1997. Shocked meteorites: Argon-40-argon-39 evidence for multiple impacts. *Meteoritics & Planetary Science* 32:647–670.

Kunz J., Trieloff M., Bobe K. D., Metzler K., Stöffler D., and Jessberger E. K. 1995. The collisional history of the HED parent body inferred from ^{40}Ar-^{39}Ar ages of eucrites. *Planetary and Space Science* 43:527–543.

Langenhorst F. and Poirier J.-P. 2000a. "Eclogitic" minerals in a shocked basaltic meteorite. *Earth and Planetary Science Letters* 176:259–265.

Langenhorst F. and Poirier J.-P. 2000b. Anatomy of black veins in Zagami: Clue to the formation of high-pressure phases. *Earth and Planetary Science Letters* 184:37–55.

Lodders K. 1998. A survey of shergottite, nakhlite, and chassigny meteorites whole-rock compositions. *Meteoritics & Planetary Science* 33:A183–A190.

Marti K., Kim J. S., Thakur A. N., McCoy T. J., and Keil K. 1995. Signatures of the Martian atmosphere in glass of the Zagami meteorite. *Science* 267:1981–1984.

Marty B., Heber V. S., Grimberg A., Wieler R., and Barrat J. A. 2006. Noble gases in the Martian meteorite Northwest Africa 2737: A new chassignite signature. *Meteoritics & Planetary Science* 41: 739–748.

Mathew K. J. and Marti K. 2001. Early evolution of Martian volatiles: Nitrogen and noble gas components in ALH 84001 and Chassigny. *Journal of Geophysical Research* 106:1401–1422.

McSween H. Y. Jr. 1994. What we have learned about Mars from SNC meteorites. *Meteoritics* 29:757–779.

McSween H. Y. Jr. and Treiman A. H. 1998. Martian meteorites. In *Planetary materials*, edited by Papike J. J. Reviews in Mineralogy, vol. 36. Washington, D.C.: Mineralogical Society of America. pp. 6-01–6-53.

Meyer C. 2006. Mars meteorite compendium. http://curator.jsc.nasa.gov/curator/antmet/mmc/mmc.htm. Accessed on October 17, 2007.

Mohapatra R. K. and Ott U. 2000. Trapped noble gases in Sayh al Uhaymir 005—A new Martian meteorite from Oman (abstract). *Meteoritics & Planetary Science* 35:A113.

Murty S. V. S. and Mohapatra R. K. 1997. Nitrogen and heavy noble gases in ALH 84001: Signatures of ancient Martian atmosphere. *Geochimica et Cosmochimica Acta* 61:5417–5428.

Nakamura N., Fujiwara T., and Nohda S. 1990. Young asteroid melting event indicated by Rb-Sr dating of the Point of Rocks meteorite. *Nature* 345:51–52.

Nishiizumi K., Okazaki R., Park J., Nagao K., Masarik J., and Finkel R. C. 2002. Exposure and terrestrial histories of Dhofar 019 Martian meteorite (abstract #1366). 33rd Lunar and Planetary Science Conference. CD-ROM.

Nyquist L. E. 2006. Martian meteorite age and implications for Martian cratering history (abstract). Workshop on Surface Ages and Histories: Issues in Planetary Chronology. LPI Contribution 1320. Houston, Texas: Lunar and Planetary Institute. pp. 39–40.

Nyquist L. E., Bansal B., Wiesmann H., and Shih C.-Y. 1995. "Martians" young and old: Zagami and ALH 84001 (abstract). 26th Lunar and Planetary Science Conference. pp. 1065–1066.

Nyquist L. E., Bogard D. D., Shih C.-Y., Greshake A., Stöffler D., and Eugster O. 2001. Ages and history of Martian meteorites. *Space Science Reviews* 96:105–164.

Nyquist L. E., Wooden J., Bansal B., Wiesmann H., McKay G. A., and Bogard D. D. 1979a. Rb-Sr age of the Shergotty achondrite and implications for the metamorphic resetting of isochron ages. *Geochimica et Cosmochimica Acta* 43:1057–1074.

Nyquist L. E., Bogard D. D., Wooden J., Wiesmann H., Shin C.-Y. and Bansal B. M. 1979b. Early differentiation, late magmatism, and recent bombardment on the shergottite parent planet (abstract). *Meteoritics* 14:502.

Nyquist L. E., Shih C.-Y., and Reese Y. D. 2006. Initial isotopic heterogeneities in Zagami: Evidence of a complex magmatic history (abstract). *Meteoritics & Planetary Science* 41:A135.

Ott U. 1988. Noble gases in SNC meteorites: Shergotty, Nakhla, Chassigny. *Geochimica et Cosmochimica Acta* 52:1937–1948.

Owen T. 1992. The composition and early history of the atmosphere of Mars. In *Mars*, edited by Kieffer H. H., Jakovsky B. M., Snyder C. W., and Matthews M. S. Tucson: The University of Arizona Press. pp. 818–834.

Park J., Okazaki R., and Nagao K. 2003. Noble gas studies of Martian meteorites: Dar al Gani 476/489, Sayh al Uhaymir 005/060, Dhofar 019, Los Angeles 001 and Zagami (abstract #1213). 34th Lunar and Planetary Science Conference. CD-ROM.

Pätsch M., Altmaier M., Herpers U., Kosuch H., Michel R., and Schultz L. 2000. Exposure age of the new SNC meteorite Sayh al Uhaymir 005 (abstract). *Meteoritics & Planetary Science* 35: A124–125.

Sano Y., Terada K., Takeno S., Taylor L. A., and McSween H. Y., Jr.

2000. Ion microprobe uranium-thorium-lead dating of Shergotty phosphates. *Meteoritics & Planetary Science* 35:341–346.

Schaeffer G. A. and Schaeffer O. A. 1977. ^{40}Ar-^{39}Ar ages of lunar rocks. Proceeding, 8th Lunar Science Conference. pp. 2253–2300.

Schwarz W. H. and Trieloff M. 2007. Intercalibration of ^{40}Ar-^{39}Ar age standards NL25, HB3gr hornblende, GA-1550, SB-3, HD-B1 biotite and BMus/2 muscovite. *Chemical Geology* 242:218–231.

Schwenzer S. P., Herrmann S., Mohapatra R. K., and Ott U. 2007. Noble gases in mineral separates from three shergottites: Shergotty, Zagami, and EETA79001. *Meteoritics & Planetary Science* 42:387–412.

Schwenzer S. P., Mohapatra R. K., Herrmann S., and Ott U. 2002. Noble gas distribution in the Martian meteorite Sayh al Uhaymir 005 (SaU 005) (abstract #1624). 33rd Lunar and Planetary Science Conference. CD-ROM.

Sharp T. G., El Goresy A., Wopenka B., and Chen M. 1999. A post-stishovite SiO$_2$ polymorph in the Shergotty meteorite: Implications for impact events. *Science* 284:1511–1513.

Shih C.-Y., Nyquist L. E., Bogard D. D., McKay G. A., Wooden J. L., Bansal B. M., and Wiesmann H. 1982. Chronology and petrogenesis of young achondrites, Shergotty, Zagami, and ALHA77005: Late magmatism on a geologically active planet. *Geochimica et Cosmochimica Acta* 46:2323–2344.

Shih Y., Nyquist L. E., and Reese Y. 2007. Rb-Sr and Sm-Nd isotopic sudies of Martian depleted shergottites SaU 094/005 (abstract #1745). 38th Lunar and Planetary Science Conference. CD-ROM.

Shukolyukov Yu. A., Nazarov M. A., and Schultz L. 2002. A new Martian meteorite: The Dhofar 019 shergottite with an exposure age of 20 million years. *Solar System Research* 36:125–135.

Steiger R. H. and Jäger E. 1977. Subcommission on geochronology: Convention on the use of decay constants in geo- and cosmochronology. *Earth and Planetary Science Letters* 36:359–362.

Stöffler D., Ostertag R., Jammes C., Pfannschmidt G., Sen Gupta P. R., Simon S. B., Papike J. J., and Beauchamp R. H. 1986. Shock metamorphism and petrography of the Shergotty achondrite. *Geochimica et Cosmochimica Acta* 50:889–903.

Stolper E. M. and McSween H. Y. Jr. 1979. Petrology and origin of the shergottite meteorites. *Geochimica et Cosmochimica Acta* 43:1475–1498.

Swindle T. D., Caffee M. W., and Hohenberg C. M. 1986. Xenon and other noble gases in shergottites. *Geochimica et Cosmochimica Acta* 50:1001–1015.

Taylor L. A., Nazarov M. A., Shearer C. K., McSween H. Y. Jr., Cahill J., Neal C. R., Ivanova M. A., and Barsukova L. D. 2002. Martian meteorite Dhofar 019: A new shergottite. *Meteoritics & Planetary Science* 37:1107–1128.

Terribilini D., Busemann H., and Eugster O. 2000. ^{81}K-K cosmic-ray exposure ages of Martian meteorites including the new shergottite Los Angeles (abstract). *Meteoritics & Planetary Science* 35:A155.

Terribilini D., Eugster O., Burger M., Jakob A., and Krähenbühl U. 1998. Noble gases and chemical composition of Shergotty mineral fractions, Chassigny, and Yamato-793605: The trapped argon-40/argon-36 ratio and ejection times of Martian meteorites. *Meteoritics & Planetary Science* 33:677–684.

Trieloff M. 1993. Datierung impaktmetamorpher Gesteine und methodische Ergänzungen zur ^{40}Ar-^{39}Ar Altersbestimmungstechnik. Ph.D. thesis, University of Heidelberg, Germany. 144 p.

Trieloff M., Deutsch A., and Jessberger E. K. 1998. The age of the Kara impact structure, Russia. *Meteoritics & Planetary Science* 33:361–372.

Trieloff M., Reimold W. U., Kunz J., Boer R. H., and Jessberger E. K. 1994a. ^{40}Ar-^{39}Ar thermochronology of pseudotachylite at the Ventersdorp Contact Reef, Witwatersrand Basin. *South African Journal of Geology* 97:365–384.

Trieloff M., Deutsch A., Kunz J., and Jessberger E. K. 1994b. Redistribution of potassium and radiogenic argon by moderate shock pressures in experimentally shocked gabbro (abstract). *Meteoritics* 29:541.

Trieloff M., Jessberger E. K., Herrwerth I., Hopp J., Fiéni C., Ghélis M., Bourot-Denise M., and Pellas P. 2003a. Structure and thermal history of the H-chondrite parent asteroid revealed by thermochronometry. *Nature* 422:502–506.

Trieloff M., Falter M., and Jessberger E. K. 2003b. The distribution of mantle and atmospheric argon in oceanic basalt glasses. *Geochimica et Cosmochimica Acta* 67:1229–1245.

Trieloff M., Weber H. W., Kurat G., Jessberger E. K., and Janicke J. 1997. Noble gases, their carrier phases, and argon chronology of upper mantle rocks from Zabargad Island, Red Sea. *Geochimica et Cosmochimica Acta* 61:5065–5088.

Treiman A. H. and Sutton S. R. 1991. Zagami: Trace-element zoning of pyroxenes by synchrotron X-ray (SXRF) microprobe, and implications for rock genesis (abstract). 22nd Lunar and Planetary Science Conference. pp. 1411–1412.

Turner G. 1971. ^{40}Ar-^{39}Ar dating: The optimization of irradiation parameters. *Earth and Planetary Science Letters* 10:227–234.

Turner G. and Cadogan P. H. 1974. Possible effects of ^{39}Ar recoil in ^{40}Ar-^{39}Ar dating. Proceedings, 5th Lunar Science Conference. pp. 1601–1615.

Walker D., Stolper E. M., and Hays J. F. 1979. Basaltic volcanism: The importance of planet size. Proceedings, 10th Lunar and Planetary Science Conference. pp. 1995–2015.

Wiens R. C. 1988. Noble gases released by vacuum crushing of EETA79001 glass. *Earth and Planetary Science Letters* 91:55–65.

Wiens R. C., Becker R. H., and Pepin R. O. 1986. The case for a Martian origin of the shergottites, II. Trapped and indigenous gas components in EETA79001 glass. *Earth and Planetary Science Letters* 77:149–158.

Zipfel J. 2000. Sayh al Uhaymir 005/008 and its relationship to Dar al Gani 476/489 (abstract). *Meteoritics & Planetary Science* 35:A178.

APPENDIX

Tables A1–A18 display measured argon isotopes corrected for mass discrimination, sensitivity, system blanks, decay, and relative neutron doses. All isotopes are also corrected for interfering isotopes produced on K and Ca during irradiation. Remaining argon isotopes are given in ccmSTP/g and have the following composition:

Apparent ages in tables were calculated by subtracting an almost negligible amount of primordial trapped argon from ^{40}Ar, assuming $^{40}Ar/^{36}Ar = 1$ in each temperature extraction.

$^{36}Ar = {}^{36}Ar_{atm} + {}^{36}Ar_{trap} + {}^{36}Ar_{cos}$	atm:	Terrestrial atmospheric argon
	trap:	Trapped extraterrestrial argon (incl. Martian atmosphere + mantle)
	cos:	Cosmogenic argon
$^{37}Ar = {}^{37}Ar_{Ca}$	Ca:	Argon derived from Ca
$^{38}Ar = {}^{38}Ar_{atm} + {}^{36}Ar_{trap} + {}^{36}Ar_{cos} + {}^{38}Ar_{Cl}$	Cl:	Argon derived from Cl
$^{39}Ar = {}^{39}Ar_{K}$	K:	Argon derived from K
$^{40}Ar = {}^{40}Ar_{rad} + {}^{40}Ar_{atm} + {}^{40}Ar_{trap}$	rad:	In situ radiogenic argon

Table A1. Dhofar 019 whole rock (122.4 mg).

Temp. (°C)	$^{36}Ar^{*}10^{-12}$	$^{37}Ar^{*}10^{-10}$	$^{38}Ar^{*}10^{-12}$	$^{39}Ar^{*}10^{-12}$	$^{40}Ar^{*}10^{-9}$	Age (Ma)
350	357 ± 10	0 ± 0	67 ± 3	5 ± 1	103 ± 3	9260 ± 440
450	3602 ± 97	3 ± 1	695 ± 19	13 ± 1	1052 ± 28	11679 ± 196
550	3204 ± 86	15 ± 1	736 ± 20	69 ± 2	947 ± 25	8507 ± 43
600	727 ± 20	40 ± 1	404 ± 11	190 ± 5	214 ± 6	4167 ± 16
650	318 ± 9	50 ± 1	282 ± 8	236 ± 7	99 ± 3	2652 ± 11
700	240 ± 7	57 ± 2	150 ± 4	185 ± 6	76 ± 2	2635 ± 14
750	547 ± 13	158 ± 4	172 ± 4	181 ± 4	167 ± 4	3849 ± 12
800	275 ± 7	187 ± 4	93 ± 3	125 ± 3	87 ± 2	3405 ± 13
850	283 ± 7	346 ± 8	116 ± 3	170 ± 4	91 ± 2	3004 ± 13
900	402 ± 10	1360 ± 31	297 ± 7	501 ± 12	157 ± 4	2265 ± 8
950	200 ± 5	795 ± 19	182 ± 5	364 ± 9	101 ± 2	2118 ± 9
1000	123 ± 4	139 ± 3	122 ± 3	213 ± 6	67 ± 2	2275 ± 14
1050	150 ± 4	205 ± 5	155 ± 4	246 ± 6	69 ± 2	2128 ± 10
1100	209 ± 6	311 ± 8	247 ± 6	352 ± 9	82 ± 2	1906 ± 6
1150	244 ± 7	342 ± 8	318 ± 8	416 ± 10	84 ± 2	1738 ± 7
1200	807 ± 19	1096 ± 25	1138 ± 25	2029 ± 45	192 ± 4	1021 ± 3
1250	594 ± 15	766 ± 18	872 ± 21	1367 ± 32	129 ± 3	1016 ± 3
1280	858 ± 21	1044 ± 25	1315 ± 31	1193 ± 28	130 ± 3	1135 ± 4
1320	1760 ± 41	2149 ± 49	2588 ± 58	2263 ± 51	227 ± 5	1066 ± 3
1360	1507 ± 37	1887 ± 45	2177 ± 52	1760 ± 42	165 ± 4	1014 ± 4
1400	820 ± 27	1058 ± 34	1184 ± 38	897 ± 28	80 ± 3	969 ± 4
1450	480 ± 40	623 ± 51	696 ± 58	400 ± 33	28 ± 2	805 ± 6
1500	2647 ± 91	3510 ± 120	3880 ± 130	2107 ± 72	132 ± 5	737 ± 5
1580	1480 ± 100	1590 ± 110	2090 ± 140	806 ± 56	77 ± 5	1027 ± 7
1650	197 ± 67	103 ± 31	174 ± 53	75 ± 23	32 ± 10	2682 ± 58
1700	74 ± 74	43 ± 43	71 ± 71	23 ± 23	9 ± 9	2630 ± 278
Total	22100 ± 230	17870 ± 200	20220 ± 250	16190 ± 140	4599 ± 43	2143 ± 48

Table A2. Dhofar 019 maskelynite (6.4 mg).

Temp. (°C)	$^{36}Ar^{*}10^{-11}$	$^{37}Ar^{*}10^{-10}$	$^{38}Ar^{*}10^{-11}$	$^{39}Ar^{*}10^{-11}$	$^{40}Ar^{*}10^{-9}$	Age (Ma)
550	4297 ± 96	29 ± 6	818 ± 18	29 ± 3	12440 ± 280	10521 ± 180
650	3462 ± 77	65 ± 6	698 ± 16	27 ± 2	10080 ± 220	10322 ± 143
750	927 ± 22	219 ± 8	205 ± 5	40 ± 3	2713 ± 61	7233 ± 120
850	2008 ± 45	1176 ± 27	414 ± 10	90 ± 3	5870 ± 130	7168 ± 42
930	54 ± 4	308 ± 14	37 ± 2	63 ± 3	159 ± 7	2001 ± 46
1000	42 ± 3	293 ± 16	41 ± 3	88 ± 5	116 ± 6	1302 ± 28
1070	56 ± 4	521 ± 24	57 ± 3	133 ± 6	136 ± 6	1087 ± 10
1150	64 ± 4	758 ± 37	85 ± 5	159 ± 8	140 ± 7	964 ± 12
1250	203 ± 6	2539 ± 68	281 ± 8	507 ± 14	362 ± 9	818 ± 5
1350	509 ± 12	5150 ± 100	605 ± 13	873 ± 18	892 ± 18	1081 ± 6
1450	552 ± 16	5150 ± 130	595 ± 16	712 ± 19	964 ± 25	1326 ± 8
1650	546 ± 63	6330 ± 660	688 ± 71	844 ± 87	773 ± 80	993 ± 5
Total	12720 ± 150	22540 ± 680	4524 ± 80	3566 ± 93	34640 ± 390	3923 ± 105

Table A3. Dhofar 019 pyroxene (14.3 mg).

Temp. (°C)	$^{36}Ar^* 10^{-11}$	$^{37}Ar^* 10^{-10}$	$^{38}Ar^* 10^{-11}$	$^{39}Ar^* 10^{-11}$	$^{40}Ar^* 10^{-9}$	Age (Ma)
450	627 ± 13	0 ± 0	117 ± 2	5 ± 1	1797 ± 36	10142 ± 309
550	2182 ± 43	19 ± 2	424 ± 8	13 ± 1	6340 ± 130	10730 ± 104
650	1372 ± 27	71 ± 2	310 ± 6	35 ± 1	4005 ± 79	8197 ± 55
750	389 ± 9	191 ± 5	107 ± 2	40 ± 1	1122 ± 23	5693 ± 35
850	1074 ± 15	1537 ± 21	227 ± 3	57 ± 1	3104 ± 41	6857 ± 36
950	90 ± 3	1296 ± 33	51 ± 2	78 ± 2	276 ± 7	2433 ± 19
1050	58 ± 3	415 ± 16	53 ± 2	115 ± 4	168 ± 6	1398 ± 11
1130	44 ± 4	463 ± 29	46 ± 3	94 ± 6	98 ± 6	1100 ± 9
1200	85 ± 5	1142 ± 61	114 ± 6	198 ± 11	138 ± 7	804 ± 6
1270	120 ± 9	1430 ± 110	167 ± 12	207 ± 15	174 ± 13	933 ± 9
1340	378 ± 22	3770 ± 210	464 ± 26	406 ± 23	501 ± 28	1241 ± 5
1410	310 ± 25	3200 ± 250	370 ± 29	217 ± 17	324 ± 25	1422 ± 11
1480	386 ± 56	4820 ± 680	533 ± 76	237 ± 34	203 ± 29	946 ± 8
1550	152 ± 69	1850 ± 820	209 ± 93	102 ± 45	99 ± 44	1039 ± 12
1650	71 ± 62	640 ± 500	75 ± 59	38 ± 30	112 ± 87	2187 ± 41
Total	7340 ± 130	20840 ± 1230	3270 ± 140	1841 ± 73	18460 ± 190	3974 ± 83

Table A4. Dhofar 019 olivine (5.1 mg).

Temp. (°C)	$^{36}Ar^* 10^{-11}$	$^{37}Ar^* 10^{-10}$	$^{38}Ar^* 10^{-11}$	$^{39}Ar^* 10^{-11}$	$^{40}Ar^* 10^{-8}$	Age (Ma)
550	3740 ± 120	11 ± 6	714 ± 22	26 ± 5	1085 ± 33	10487 ± 318
650	2752 ± 87	25 ± 8	558 ± 18	42 ± 4	803 ± 25	9111 ± 142
750	837 ± 28	205 ± 10	189 ± 6	57 ± 3	246 ± 8	6451 ± 86
850	2223 ± 70	2491 ± 78	455 ± 14	78 ± 4	647 ± 20	7610 ± 68
950	49 ± 6	984 ± 72	32 ± 3	65 ± 5	21 ± 2	2293 ± 42
1050	65 ± 7	381 ± 27	41 ± 4	93 ± 7	26 ± 2	2096 ± 36
1150	58 ± 9	460 ± 50	46 ± 6	77 ± 9	19 ± 2	1999 ± 39
1250	95 ± 14	752 ± 82	102 ± 12	127 ± 14	27 ± 3	1778 ± 22
1350	310 ± 21	2040 ± 120	324 ± 20	277 ± 17	63 ± 4	1878 ± 14
1450	245 ± 35	1090 ± 140	216 ± 27	78 ± 10	41 ± 5	2975 ± 49
1550	271 ± 73	1010 ± 240	252 ± 61	88 ± 21	41 ± 10	2789 ± 50
1650	140 ± 140	160 ± 120	75 ± 61	33 ± 26	32 ± 25	3900 ± 297
Total	10780 ± 230	9600 ± 360	3005 ± 99	1042 ± 44	3050 ± 54	5771 ± 169

Table A5. Dhofar 019 opaque (0.1 mg).

Temp. (°C)	$^{36}Ar^* 10^{-9}$	$^{37}Ar^* 10^{-8}$	$^{38}Ar^* 10^{-9}$	$^{39}Ar^* 10^{-10}$	$^{40}Ar^* 10^{-7}$	Age (Ma)
450	1347 ± 44	2 ± 2	252 ± 8	150 ± 16	3840 ± 130	9613 ± 178
650	3320 ± 110	13 ± 4	631 ± 21	20 ± 20	9670 ± 310	14917 ± 1775
850	1515 ± 50	92 ± 4	296 ± 10	220 ± 18	4350 ± 140	9148 ± 135
1050	48 ± 4	21 ± 3	12 ± 1	35 ± 11	152 ± 8	6482 ± 564
1250	44 ± 7	35 ± 5	17 ± 2	99 ± 16	130 ± 14	4420 ± 204
1450	155 ± 14	112 ± 9	60 ± 5	175 ± 17	411 ± 28	5391 ± 119
1650	29 ± 29	30 ± 30	19 ± 19	8 ± 8	81 ± 81	7987 ± 1499
Total	6460 ± 130	305 ± 32	1287 ± 31	707 ± 41	18630 ± 380	9669 ± 1265

Table A6. SaU 005 whole rock (50.1 mg).

Temp. (°C)	$^{36}Ar^*10^{-12}$	$^{37}Ar^*10^{-10}$	$^{38}Ar^*10^{-12}$	$^{39}Ar^*10^{-12}$	$^{40}Ar^*10^{-10}$	Age (Ma)
500	20 ± 2	15 ± 5	5 ± 1	3 ± 2	48 ± 2	4732 ± 1153
600	339 ± 10	4 ± 4	129 ± 4	15 ± 2	964 ± 28	7184 ± 253
680	271 ± 8	35 ± 6	525 ± 16	162 ± 5	811 ± 23	2893 ± 18
740	112 ± 4	58 ± 6	187 ± 6	137 ± 5	344 ± 10	1976 ± 27
800	263 ± 8	466 ± 18	191 ± 6	202 ± 7	833 ± 24	2620 ± 22
860	252 ± 9	643 ± 22	306 ± 9	374 ± 11	921 ± 27	1952 ± 12
900	59 ± 3	94 ± 5	93 ± 2	204 ± 4	341 ± 5	1521 ± 14
940	30 ± 2	94 ± 4	52 ± 1	190 ± 4	283 ± 4	1409 ± 12
990	32 ± 2	180 ± 8	63 ± 2	349 ± 7	338 ± 5	1027 ± 9
1040	32 ± 2	296 ± 11	60 ± 3	469 ± 8	354 ± 5	845 ± 6
1100	33 ± 2	326 ± 8	60 ± 2	480 ± 8	338 ± 5	800 ± 5
1150	37 ± 2	353 ± 11	60 ± 2	532 ± 9	327 ± 5	715 ± 4
1200	64 ± 2	857 ± 15	116 ± 3	1244 ± 19	642 ± 9	618 ± 4
1240	65 ± 2	741 ± 16	133 ± 3	765 ± 12	462 ± 7	706 ± 4
1280	98 ± 5	1081 ± 38	154 ± 6	840 ± 29	607 ± 21	817 ± 6
1320	124 ± 6	1408 ± 51	153 ± 6	898 ± 33	704 ± 25	872 ± 6
1360	73 ± 7	860 ± 52	82 ± 5	519 ± 31	350 ± 21	771 ± 6
1400	87 ± 11	1426 ± 99	128 ± 9	907 ± 63	466 ± 33	616 ± 5
1450	55 ± 21	910 ± 250	78 ± 22	370 ± 100	172 ± 47	568 ± 9
1500	233 ± 39	2180 ± 280	255 ± 33	737 ± 94	664 ± 85	971 ± 9
Total	2277 ± 51	12020 ± 400	2831 ± 47	9390 ± 160	9970 ± 120	1101 ± 18

Table A7. SaU 005 glass (14.1 mg).

Temp. (°C)	$^{36}Ar^*10^{-12}$	$^{37}Ar^*10^{-9}$	$^{38}Ar^*10^{-12}$	$^{39}Ar^*10^{-12}$	$^{40}Ar^*10^{-9}$	Age (Ma)
600	1356 ± 34	0 ± 0	449 ± 14	133 ± 11	387 ± 9	5745 ± 132
700	755 ± 21	6 ± 2	262 ± 9	181 ± 9	224 ± 5	4292 ± 75
800	4280 ± 100	52 ± 2	973 ± 24	328 ± 11	1272 ± 29	6235 ± 45
860	946 ± 23	9 ± 2	237 ± 9	260 ± 9	344 ± 8	4405 ± 39
900	143 ± 7	3 ± 3	52 ± 6	88 ± 6	73 ± 2	3662 ± 105
960	188 ± 9	4 ± 2	63 ± 7	153 ± 7	116 ± 3	3512 ± 57
1040	264 ± 10	12 ± 2	84 ± 4	267 ± 10	170 ± 4	3247 ± 45
1100	416 ± 13	16 ± 3	107 ± 7	289 ± 11	212 ± 5	3466 ± 46
1150	391 ± 12	23 ± 3	117 ± 5	340 ± 10	223 ± 5	3287 ± 31
1190	259 ± 9	22 ± 2	82 ± 5	258 ± 8	188 ± 4	3452 ± 33
1220	218 ± 8	33 ± 2	96 ± 4	234 ± 10	184 ± 4	3568 ± 53
1260	303 ± 11	42 ± 6	105 ± 10	298 ± 11	297 ± 7	3945 ± 49
1300	394 ± 16	70 ± 3	165 ± 7	380 ± 11	455 ± 10	4237 ± 31
1340	564 ± 20	77 ± 3	179 ± 6	378 ± 10	507 ± 8	4425 ± 35
1380	1523 ± 37	209 ± 5	529 ± 13	660 ± 15	1592 ± 21	5414 ± 31
1420	614 ± 41	80 ± 4	237 ± 13	232 ± 9	623 ± 14	5598 ± 52
1460	398 ± 57	45 ± 4	135 ± 14	150 ± 12	355 ± 17	5389 ± 106
1500	0 ± 0	0 ± 0	0 ± 0	0 ± 0	0 ± 0	0 ± 0
1640	1730 ± 310	54 ± 6	479 ± 69	195 ± 22	737 ± 76	6192 ± 78
Total	14740 ± 340	758 ± 14	4353 ± 81	4824 ± 47	7960 ± 90	4771 ± 20

Table A8. SaU 005 maskelynite (0.6 mg).

Temp. (°C)	$^{36}Ar^*10^{-10}$	$^{37}Ar^*10^{-9}$	$^{38}Ar^*10^{-10}$	$^{39}Ar^*10^{-10}$	$^{40}Ar^*10^{-8}$	Age (Ma)
600	105 ± 3	1 ± 1	24 ± 1	4 ± 2	304 ± 5	7432 ± 858
800	77 ± 3	60 ± 31	27 ± 2	8 ± 1	222 ± 5	5608 ± 288
1000	232 ± 4	95 ± 25	57 ± 2	25 ± 2	668 ± 10	5575 ± 122
1200	83 ± 3	311 ± 24	20 ± 1	55 ± 2	249 ± 6	2740 ± ± 37
1400	50 ± 5	1099 ± 71	21 ± 2	133 ± 8	202 ± 12	1426 ± 21
1600	20 ± 17	910 ± 460	15 ± 8	60 ± 30	83 ± 41	1344 ± 32
Total	568 ± 19	2480 ± 460	163 ± 9	285 ± 31	1728 ± 45	3171 ± 223

Table A9. SaU 005 pyroxene (0.3 mg).

Temp. (°C)	$^{36}Ar^*10^{-10}$	$^{37}Ar^*10^{-8}$	$^{38}Ar^*10^{-10}$	$^{39}Ar^*10^{-11}$	$^{40}Ar^*10^{-7}$	Age (Ma)
600	437 ± 20	5 ± 5	92 ± 5	100 ± 24	126 ± 5	8323 ± 424
800	334 ± 16	27 ± 5	62 ± 4	3 ± 3	95 ± 4	13979 ± 19668
1000	230 ± 11	17 ± 6	57 ± 4	358 ± 32	67 ± 3	4987 ± 133
1200	87 ± 6	0 ± 0	18 ± 3	224 ± 32	25 ± 2	4115 ± 206
1400	135 ± 14	60 ± 8	49 ± 5	417 ± 50	39 ± 3	3839 ± 138
1600	390 ± 47	27 ± 9	84 ± 10	233 ± 42	117 ± 11	6680 ± 265
1800	160 ± 150	7 ± 7	35 ± 31	300 ± 210	47 ± 33	4673 ± 206
Total	1780 ± 160	143 ± 17	398 ± 34	1640 ± 230	515 ± 36	5874 ± 4901

Table A10. SaU 005 olivine (13.1 mg).

Temp. (°C)	$^{36}Ar^*10^{-11}$	$^{37}Ar^*10^{-9}$	$^{38}Ar^*10^{-11}$	$^{39}Ar^*10^{-12}$	$^{40}Ar^*10^{-9}$	Age (Ma)
800	119 ± 3	58 ± 2	88 ± 2	559 ± 17	357 ± 9	3251 ± 27
1000	147 ± 4	57 ± 2	74 ± 2	896 ± 25	464 ± 11	2942 ± 21
1200	33 ± 2	119 ± 4	27 ± 1	1768 ± 56	190 ± 6	1112 ± 7
1400	103 ± 3	599 ± 17	76 ± 2	4050 ± 110	505 ± 14	1239 ± 4
1600	111 ± 7	535 ± 25	61 ± 3	1649 ± 77	370 ± 17	1842 ± 12
1780	170 ± 29	13 ± 2	33 ± 6	34 ± 8	487 ± 61	8542 ± 352
Total	683 ± 30	1381 ± 31	359 ± 8	8960 ± 150	2373 ± 67	2040 ± 77

Table A11. Shergotty whole rock (50.2 mg).

Temp. (C)	$^{36}Ar^*10^{-12}$	$^{37}Ar^*10^{-10-}$	$^{38}Ar^*10^{-12}$	$^{39}Ar^*10^{-12}$	$^{40}Ar^*10^{-10}$	Age (Ma)
300	22 ± 2	0 ± 0	6 ± 2	10 ± 2	59 ± 5	3066 ± 315
450	24 ± 2	0 ± 0	1 ± 1	13 ± 3	69 ± 5	2975 ± 301
550	29 ± 4	0 ± 0	7 ± 2	14 ± 4	77 ± 9	3036 ± 358
650	53 ± 2	17 ± 1	110 ± 4	1308 ± 27	458 ± 9	443 ± 1.5
750	146 ± 3	56 ± 1	277 ± 5	7275 ± 77	1992 ± 21	355 ± 0.7
850	217 ± 4	146 ± 2	527 ± 6	10780 ± 110	4089 ± 39	475 ± 1.0
950	235 ± 4	260 ± 3	727 ± 8	10680 ± 110	3421 ± 33	409 ± 0.7
1050	267 ± 4	739 ± 8	1734 ± 19	12680 ± 130	3621 ± 37	369 ± 0.7
1150	302 ± 5	1041 ± 12	1551 ± 18	11270 ± 120	3306 ± 36	378 ± 0.8
1250	523 ± 8	2664 ± 31	1386 ± 17	12710 ± 140	4061 ± 45	408 ± 1.0
1350	1152 ± 18	6224 ± 73	1821 ± 22	12650 ± 140	4806 ± 57	476 ± 1.9
1450	1043 ± 20	4856 ± 86	1003 ± 18	5170 ± 92	2788 ± 51	643 ± 4
1550	982 ± 36	1317 ± 47	419 ± 16	2623 ± 93	2736 ± 97	1089 ± 4
1650	670 ± 160	299 ± 69	155 ± 38	1340 ± 310	1160 ± 270	946 ± 10
1700	1010 ± 200	28 ± 6	174 ± 38	214 ± 47	1760 ± 350	3637 ± 152
Total	6670 ± 260	17650 ± 140	9897 ± 72	88730 ± 470	34400 ± 470	484 ± 5

Table A12. Shergotty glass (3.8 mg).

Temp. (°C)	$^{36}Ar^*10^{-11}$	$^{37}Ar^*10^{-10-}$	$^{38}Ar^*10^{-11}$	$^{39}Ar^*10^{-11}$	$^{40}Ar^*10^{-8}$	Age (Ma)
650	38 ± 7	19 ± 4	16 ± 3	61 ± 7	15 ± 2	1958 ± 48
850	161 ± 7	330 ± 10	131 ± 4	1442 ± 26	220 ± 4	1433 ± 7
1050	792 ± 16	2234 ± 36	352 ± 8	1768 ± 29	1195 ± 18	3340 ± 9
1250	1275 ± 24	5017 ± 80	671 ± 12	2494 ± 39	1937 ± 29	3554 ± 6
1450	2315 ± 52	8500 ± 130	959 ± 17	3615 ± 57	3471 ± 53	3887 ± 7
1550	171 ± 92	550 ± 74	78 ± 20	364 ± 49	199 ± 27	3023 ± 14
1650	170 ± 160	480 ± 100	70 ± 32	353 ± 76	211 ± 45	3156 ± 17
Total	4920 ± 190	17120 ± 210	2277 ± 44	10100 ± 120	7249 ± 82	3432 ± 6

Table A13. Shergotty maskelynite (8.7 mg).

Temp. (°C)	$^{36}Ar^*10^{-11}$	$^{37}Ar^*10^{-10}$	$^{38}Ar^*10^{-12}$	$^{39}Ar^*10^{-11}$	$^{40}Ar^*10^{-9}$	Age (Ma)
450	2 ± 2	10 ± 9	5 ± 5	8 ± 7	9 ± 8	1162 ± 108
550	8 ± 4	3 ± 2	17 ± 13	4 ± 2	23 ± 8	3274 ± 534
650	7 ± 3	21 ± 3	82 ± 25	136 ± 19	61 ± 8	547 ± 6
750	8 ± 3	61 ± 4	164 ± 16	450 ± 24	191 ± 10	524 ± 3
850	42 ± 3	328 ± 11	498 ± 21	935 ± 30	651 ± 21	794 ± 2
920	44 ± 3	466 ± 15	456 ± 20	946 ± 30	720 ± 23	853 ± 2
980	33 ± 4	534 ± 19	469 ± 21	901 ± 31	559 ± 19	722 ± 2
1040	37 ± 3	844 ± 29	649 ± 27	1109 ± 38	574 ± 20	621 ± 1.8
1100	35 ± 4	1105 ± 39	657 ± 27	1183 ± 42	554 ± 19	570 ± 1.6
1160	29 ± 4	997 ± 52	475 ± 30	868 ± 45	337 ± 17	484 ± 1.4
1250	77 ± 6	3790 ± 160	1350 ± 62	2650 ± 110	890 ± 38	426 ± 1.2
1350	120 ± 8	5670 ± 240	1761 ± 79	4000 ± 170	1217 ± 52	391 ± 0.8
1450	65 ± 13	2070 ± 180	678 ± 64	1390 ± 120	478 ± 42	436 ± 1.0
1550	7 ± 7	1870 ± 580	540 ± 190	1250 ± 390	380 ± 120	393 ± 1.4
1650	0 ± 0	1890 ± 1890	440 ± 440	1150 ± 1150	110 ± 110	134 ± 0.9
1700	0 ± 0	0 ± 0	0 ± 0	0 ± 0	0 ± 0	0 ± 0
Total	514 ± 21	19650 ± 2010	8240 ± 490	16980 ± 1240	6760 ± 190	496 ± 42

Table A14. Shergotty pyroxene (15.6 mg).

Temp. (°C)	$^{36}Ar^*10^{-11}$	$^{37}Ar^*10^{-10}$	$^{38}Ar^*10^{-11}$	$^{39}Ar^*10^{-11}$	$^{40}Ar^*10^{-9}$	Age (Ma)
450	1 ±	2 ± 2	2 ± 2	5 ± 5	4 ± 4	796 ± 94
550	3 ± 3	3 ± 2	4 ± 3	4 ± 2	10 ± 6	1974 ± 208
650	2 ± 2	7 ± 3	2 ± 1	22 ± 8	16 ± 6	850 ± 24
750	5 ± 2	30 ± 3	11 ± 1	252 ± 20	82 ± 6	412 ± 2
850	17 ± 2	63 ± 2	18 ± 1	349 ± 10	206 ± 6	693 ± 3
950	32 ± 2	143 ± 3	25 ± 1	192 ± 4	343 ± 6	1593 ± 8
1050	22 ± 2	175 ± 7	23 ± 1	89 ± 3	172 ± 6	1679 ± 10
1150	24 ± 3	453 ± 23	25 ± 2	64 ± 3	150 ± 8	1891 ± 15
1250	48 ± 4	2033 ± 92	50 ± 3	62 ± 3	226 ± 10	2443 ± 22
1350	117 ± 8	4870 ± 220	95 ± 4	41 ± 2	345 ± 15	3688 ± 49
1450	87 ± 13	2880 ± 320	59 ± 7	21 ± 3	216 ± 24	3966 ± 84
1550	87 ± 31	4310 ± 1190	78 ± 22	12 ± 4	207 ± 57	4813 ± 250
1650	81 ± 57	1440 ± 720	38 ± 21	7 ± 4	230 ± 120	6064 ± 793
Total	527 ± 67	16400 ± 1450	432 ± 32	1121 ± 27	2210 ± 130	1697 ± 99

Table A15. Zagami whole rock (56.0 mg).

Temp. (°C)	$^{36}Ar^*10^{-12}$	$^{37}Ar^*10^{-10}$	$^{38}Ar^*10^{-12}$	$^{39}Ar^*10^{-12}$	$^{40}Ar^*10^{-9}$	Age (Ma)
450	5 ± 5	0 ± 0	2 ± 2	3 ± 3	1 ± 1	2718 ± 810
550	12 ± 5	0 ± 0	3 ± 2	0 ± 0	4 ± 1	0 ± 0
650	27 ± 4	10 ± 1	37 ± 3	487 ± 34	16 ± 1	410 ± 2
750	64 ± 4	64 ± 2	254 ± 8	8710 ± 250	155 ± 4	238 ± 0.5
850	242 ± 8	187 ± 5	711 ± 21	19830 ± 550	478 ± 13	316 ± 0.5
950	189 ± 7	472 ± 13	1038 ± 30	17570 ± 490	350 ± 10	265 ± 0.4
1050	241 ± 7	1002 ± 17	1187 ± 20	14800 ± 250	278 ± 5	251 ± 0.6
1150	234 ± 7	953 ± 17	886 ± 16	9060 ± 160	192 ± 3	280 ± 0.7
1250	536 ± 12	2948 ± 51	1272 ± 22	7680 ± 130	243 ± 4	405 ± 1.5
1350	1839 ± 35	10770 ± 180	2417 ± 42	9960 ± 170	418 ± 8	519 ± 3.7
1450	940 ± 25	5790 ± 130	1114 ± 25	4256 ± 96	195 ± 5	559 ± 4.7
1550	320 ± 40	263 ± 22	119 ± 12	785 ± 66	107 ± 9	1320 ± 7.7
1650	730 ± 100	138 ± 13	171 ± 21	146 ± 15	222 ± 21	4641 ± 72
1700	250 ± 150	30 ± 13	66 ± 35	26 ± 14	75 ± 32	5733 ± 583
Total	5630 ± 190	22630 ± 230	9277 ± 82	93310 ± 870	2733 ± 45	377 ± 7

Table A16. Zagami maskelynite (11.4 mg).

Temp. (°C)	$^{36}Ar^*10^{-11}$	$^{37}Ar^*10^{-10}$	$^{38}Ar^*10^{-11}$	$^{39}Ar^*10^{-11}$	$^{40}Ar^*10^{-9}$	Age (Ma)
650	16 ± 3	10 ± 2	6 ± 2	39 ± 5	54 ± 7	1344 ± 18
750	7 ± 3	51 ± 6	10 ± 2	241 ± 25	68 ± 7	367 ± 2
830	9 ± 3	98 ± 6	19 ± 1	434 ± 26	122 ± 7	363 ± 1.5
900	24 ± 3	287 ± 10	34 ± 2	615 ± 20	246 ± 8	498 ± 2
960	33 ± 3	516 ± 15	52 ± 2	775 ± 22	294 ± 8	475 ± 1.6
1020	32 ± 3	673 ± 20	62 ± 2	936 ± 27	287 ± 8	393 ± 1.1
1100	31 ± 3	860 ± 30	64 ± 3	1027 ± 35	285 ± 10	359 ± 1.0
1170	21 ± 4	874 ± 45	64 ± 4	941 ± 48	229 ± 12	319 ± 0.8
1250	36 ± 5	1895 ± 84	85 ± 4	1670 ± 74	360 ± 16	286 ± 0.9
1350	83 ± 8	4580 ± 130	156 ± 5	3670 ± 100	751 ± 21	272 ± 0.8
1450	43 ± 12	3110 ± 230	99 ± 8	2550 ± 190	470 ± 35	247 ± 0.8
1550	7 ± 7	2100 ± 570	68 ± 19	1730 ± 470	252 ± 68	198 ± 0.7
1650	11 ± 11	2630 ± 890	82 ± 28	2150 ± 730	330 ± 110	206 ± 0.7
1700	0 ± 0	0 ± 0	0 ± 0	0 ± 0	0 ± 0	0 ± 0
Total	351 ± 22	17690 ± 1090	800 ± 36	16790 ± 900	3740 ± 140	295 ± 5

Table A17. Zagami pyroxene (16.5 mg).

Temp. (°C)	$^{36}Ar^*10^{-11}$	$^{37}Ar^*10^{-10}$	$^{38}Ar^*10^{-11}$	$^{39}Ar^*10^{-12}$	$^{40}Ar^*10^{-9}$	Age (Ma)
550	13 ± 2	1 ± 1	5 ± 1	38 ± 7	39 ± 5	3956 ± 232
650	6 ± 2	17 ± 3	7 ± 1	629 ± 95	33 ± 5	624 ± 5
750	3 ± 2	47 ± 3	15 ± 1	4630 ± 240	102 ± 5	290 ± 1.3
850	13 ± 2	76 ± 3	26 ± 1	6850 ± 180	227 ± 6	422 ± 0.8
950	18 ± 2	208 ± 5	38 ± 1	4760 ± 110	309 ± 7	751 ± 3
1050	8 ± 2	252 ± 20	35 ± 3	1480 ± 120	65 ± 5	539 ± 4
1150	7 ± 2	424 ± 70	27 ± 5	770 ± 130	37 ± 6	586 ± 5
1250	32 ± 4	2250 ± 180	60 ± 5	1430 ± 110	104 ± 8	823 ± 6
1350	89 ± 9	6060 ± 510	114 ± 10	1119 ± 96	145 ± 12	1277 ± 17
1450	95 ± 50	8250 ± 4280	141 ± 73	580 ± 300	47 ± 25	906 ± 43
1550	89 ± 37	6400 ± 2480	112 ± 44	710 ± 280	92 ± 36	1278 ± 33
1650	33 ± 30	440 ± 280	8 ± 8	11 ± 11	95 ± 61	7707 ± 4251
Total	407 ± 70	24420 ± 4990	587 ± 87	23010 ± 570	1295 ± 78	667 ± 140

Table A18. Zagami opaque (0.9 mg).

Temp. (°C)	$^{36}Ar^*10^{-10}$	$^{37}Ar^*10^{-9}$	$^{38}Ar^*10^{-10}$	$^{39}Ar^*10^{-10}$	$^{40}Ar^*10^{-8}$	Age (Ma)
650	40 ± 3	6 ± 1	14 ± 1	34 ± 2	130 ± 7	2519 ± 57
850	59 ± 3	48 ± 3	26 ± 1	209 ± 6	294 ± 8	1354 ± 7
1050	67 ± 3	145 ± 4	35 ± 2	90 ± 2	529 ± 11	3136 ± 21
1250	68 ± 4	373 ± 10	36 ± 1	64 ± 2	683 ± 15	4050 ± 27
1450	196 ± 16	596 ± 19	71 ± 4	70 ± 3	1680 ± 52	5403 ± 31
1650	532 ± 90	94 ± 12	107 ± 18	1 ± 1	1620 ± 190	12845 ± 5760
Total	963 ± 92	1262 ± 25	288 ± 18	468 ± 8	4930 ± 200	4035 ± 2374